Calcium Concentration and Movement in the Ventricular Cardiac Cell during an Excitation-Contraction Cycle

A. Peskoff* and G. A. Langer*[#]

Cardiovascular Research Laboratory and Departments of *Physiology and [#]Medicine, UCLA School of Medicine, Los Angeles, California 90095-1760 USA

ABSTRACT   This paper extends the model for Ca movement in the cardiac ventricular cell from the diadic cleft space to the entire sarcomere. The model predicts the following: 1) Shortly after SR release there is a [Ca] gradient >3 orders of magnitude from cleft center to M-line which, 50 ms after release, is still >30. Outside the cleft, 40 ms after cessation of release, the axial gradient from Z to M-line is >3. 2) At the end of SR release, >50% of the total Ca released is bound to low-affinity inner sarcolemmal phospholipid binding sites within the cleft. 3) Halving the SR release almost doubles the fraction of release removed from the cell via Na/Ca exchange and reduces average sarcomeric free [Ca] by 70%. 4) Adding 100 μM fluo-3, which doubles the buffering capacity of the cytoplasm, reduces peak average sarcomeric [Ca] by >50% and increases the initial half-time for [Ca] decrease by approximately twofold. 5) A typical Ca "spark" can be generated by an SR release 20% of maximum (4×10^{-20} moles) over 2 ms. Fluo-3 (100 μM) significantly "shrinks" the spark. 6) The "spark" is a consequence of elementary events within the diadic cleft space. For example, removal of cleft binding sites would cause average sarcomeric Ca to increase by >10 fold, fall 10 times more rapidly, decrease latency for appearance of the spark by >20 times, and reduce spark duration by 85%. 7) Dividing SR Ca release between cleft and corbular SR produces a secondary [Ca] peak and a "flattening" of the sarcomeric [Ca] transient. These changes probably could not be resolved with current confocal microscopic techniques.

INTRODUCTION

We have previously modeled (Peskoff et al., 1992; Langer and Peskoff, 1996) the diffusion and binding of Ca in the region of the cell between the lateral cistern of the sarcoplasmic reticulum (SR) and the inner sarcolemmal (SL) membrane in cardiac ventricular cells. We have designated this region the "diadic cleft." In the earlier model, Ca is assumed to enter the diadic cleft from the SR "feet," from the Ca channel and/or via "reverse" Na/Ca exchange. Subsequently, most of this Ca diffuses from the cleft to the sarcoplasm, with a small fraction transported from the cell by Na/Ca exchange. Both components are markedly affected by Ca binding on the inner sarcolemmal surface (Post and Langer, 1992; Peskoff et al., 1992; Langer and Peskoff, 1996). In the computation, the boundary condition at the outer border of the cleft was assumed fixed at 100 nM. This did not introduce any significant error because the much higher, millimolar values of [Ca] that were predicted in the interior of the cleft were insensitive to the [Ca] assumed at the boundary, as long as it was small compared to the computed [Ca] inside the cleft.

In the present paper, we extend the model beyond the cleft into the remainder of the sarcomere, where [Ca] is in the micromolar range. The [Ca] at the cleft border, along with the [Ca] beyond the border in the sarcomere outside the cleft, now must be computed. The fixed 100 nM boundary

condition of the earlier model is replaced by the condition that the [Ca] is continuous across the border, and the Ca flux leaving the cleft equals the Ca flux entering the region of the sarcomere beyond the cleft. Except for this change in the boundary condition, the region inside the cleft, assumed to have the idealized shape of a circular disk of 200 nm radius, is modeled as earlier. The one-half sarcomere is assumed to be a circular cylinder of 500-nm radius, 1000 nm length (Z-line to M-line), with the cleft disk located coaxially at the Z-line. In the region outside the cleft it is assumed that the magnitude of the Ca diffusion coefficient is between that of free solution and that in the cleft. Outside the cleft, the diffusion equation is coupled to the kinetic equations for binding to calmodulin and troponin, and when present, to the fluorescent dye fluo-3, using experimental values for the forward and backward rate constants. Inside the cleft, as earlier, we treat the binding reactions as instantaneous. We assume zero flux leaving the sarcomere through its ends or its cylindrical surface. Reuptake by the longitudinal SR is assumed to occur just inside the cylindrical surface of the sarcomere.

The computed spatial and temporal distribution of Ca allows us to relate an observed Ca distribution in the sarcomere to a particular source within the cleft. We also relate [Ca] measurements using fluorescent dyes to the condition without dye. We find that the concentrations predicted by the computation, particularly close to the border of the cleft, are considerably higher than have been observed. This can be explained by the lowering of the [Ca] by the presence of dye, the finite response time of the fluorescence, and the limited spatial resolution of the measurements. We also gain insight into the origin of measured Ca "sparks" by setting

---

the magnitude of release by a ryanodine receptor within the cleft to yield a response in the sarcomere resembling the spark magnitude and configuration.

Initially we assume an SR Ca release sufficient to produce maximum force development (Fabiato, 1985). This is 2×10^{-19} moles/cleft, which represents >150 μmol Ca/liter accessible cell water. This Ca is released over 10 ms from a source equivalent to a single ryanodine receptor (Cheng et al., 1996) at the center of the diadic cleft space. The subsequent Ca concentration, [Ca], is followed inside the cleft and in both radial and axial directions over the half-sarcomere (0.5 μm radius; 1 μm to the M-line) for 200 ms. In addition, we take simultaneous "snapshots" of free [Ca] and total Ca as it exists in the sarcomere at selected times (5, 10, 20, 50 ms) after release. These "snapshots" are three-dimensional representations of intrasarcomere [Ca], as might be revealed by high-speed digital imaging microscopy (Isenberg et al., 1996). We then calculate the percentage of SR Ca release that diffuses to the cytoplasm from the cleft; is exchanged via Na/Ca exchange, and is free and bound in the cleft over the 200 ms after release. Similarly, we also calculate the percentage of Ca entering the sarcomere from the cleft which is free, bound to troponin and calmodulin, and resequestered by the SR over the same time period. All of these distributions assume a 10-ms SR Ca release of 2×10^{-19} moles Ca at the cleft center. We then reduce the 10-ms release by 50% to 1×10^{-19} moles which, according to Fabiato (1985), would produce about 30% maximum force. We illustrate the effect of this reduction on [Ca] in the radial and axial directions and on the instantaneous intrasarcomeric distribution, as previously.

Finally, we examine a number of special cases: 1) the effect of adding 100 μM fluo-3 (Minta et al., 1989; Kao et al., 1989) on the sarcomeric [Ca] profile; 2) the [Ca] profile in the cleft and sarcomere after a 1-ms 0.3 pA Ca entry into the cleft center from a Ca channel (this is a revision of Langer and Peskoff, 1996); 3) SR Ca release of an amount (4×10^{-20} moles) and duration (2 ms) predicted to produce a sarcomeric "Ca spark" (Santana et al., 1996; Cheng et al., 1996) in both the absence and presence of fluo-3 (the [Ca] profiles in the cleft and sarcomere are followed for 50 ms after the time of release); 4) the effect on the cleft and sarcomeric [Ca] profiles of dividing 2×10^{-19} moles Ca release equally between cleft center and corbular SR (CSR) placed at the sarcomere outer boundary at an axial distance 400 nm from the cleft (Jorgensen et al., 1985; Dolber and Sommer, 1984).

MATHEMATICAL MODEL

Geometry of the sarcomere

The "diadic cleft" is the narrow region between the lateral cistern of the sarcoplasmic reticulum (SR) and the inner sarcolemmal membrane (SL) of a cardiac cell. It contains "L" Ca channels, through which Ca enters from the interstitium, and the "feet" of the SR, from which Ca is released.

The feet occupy about two-thirds of the volume of the cleft (Wibo et al., 1991; Langer and Peskoff, 1996). The SL contains Ca-binding sites of both low and high affinity (Post and Langer, 1992) and Na/Ca exchangers (Frank et al., 1992). In the present paper we extend our earlier model for Ca movement inside the diadic cleft to compute the [Ca] as it varies with position and time not only inside the cleft, but also on the boundary of the cleft, and in the remainder of the sarcomere outside the cleft. We use cylindrical coordinates (r, z) with the plane of the Z-line at $z = 0$ (Fig. 1). There is a half-sarcomere extending from the Z-line to an adjacent M-line, and its mirror image (not shown in Fig. 1) is extending to the M-line in the opposite direction. Ca diffusing out of the cleft splits equally between the two half-sarcomeres. The half-sarcomere is modeled as a circular cylinder of radius $b = 0.5$ μm and length $l = 1.0$ μm. The cleft, which is modeled as earlier (Langer and Peskoff, 1996), as a circular disk of radius $a = 0.2$ μm and thickness $h = 12$ nm, is located at a Z-line with its center at $(r, z) = (0, 0)$, coaxial with the sarcomere.

The cleft is actually wrapped around a T-tubule and is irregular in shape; in the model it is assumed to be flattened into a circular disc of uniform thickness straddling the plane of the Z-line. We limit our consideration to rotationally symmetrical cases (independent of the azimuthal angle). Because diffusion across the transverse dimension a of the cleft is orders of magnitude slower than diffusion across the longitudinal dimension h (partly because $h \ll a$ and partly
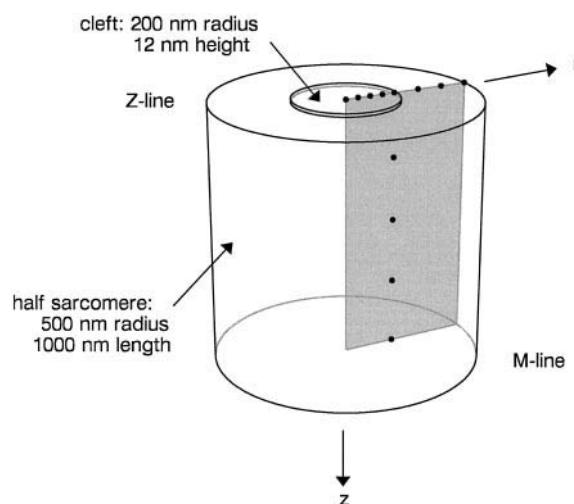

FIGURE 1   Geometry of the model, showing one-half of a sarcomere extending from a Z-line to an adjacent M-line. The position in the sarcomere is expressed in cylindrical coordinates (r, z), with the plane of the Z-line defined as $z = 0$. The half-sarcomere is modeled as a circular cylinder of radius $b = 0.5$ μm and length $l = 1.0$ μm; the cleft is modeled as a coaxial circular disk of radius $a = 0.2$ μm and thickness $h = 12$ nm, with its center at $(r, z) = (0, 0)$. The eight points shown in the $z = 0$ plane at differing radial locations (four points inside the cleft, one point on the cleft boundary, and three points outside the cleft) and the five points shown at $r = a = 200$ nm at differing axial locations are points at which graphs of [Ca] versus time will be shown. The shaded plane is the surface over which 3-D snapshots of the spatial distribution of [Ca] in the sarcomere outside the cleft will be shown.

because of the slowing of Ca movement in the r-direction by the presence of the SL binding sites), it is permissible to ignore the z-dependence and consider [Ca] within the cleft to be dependent only on the radial coordinate, r, and time, t. Outside the cleft it depends on r, z, and t.

The region of the sarcomere outside the cleft is modeled as a homogeneous medium with an effective diffusion coefficient lower than in free aqueous solution, but higher than in the cleft. Beyond lowering of the effective diffusion coefficient, the specific effects of geometric obstructions to Ca movement, for example, the mitochondria, are ignored. In particular, the volume occupied by the cleft itself, which extends 6 nm into each half of the sarcomere, is ignored, so that, for $|z| < 6$ nm and $0 \leq r \leq 200$ nm, there is one value of [Ca] inside the cleft, denoted $U(r, t)$, and one value outside the cleft, denoted $C_0(r, z, t)$.

For the finite-difference computation, the region inside the cleft is divided into 80 annular elements. The continuous radial variable r is replaced by the discrete variable $r_i = i\Delta r_{cleft}$, with $0 \leq i \leq 80$ and $\Delta r_{cleft} = 2.5$ nm. The region outside the cleft is divided into 20 annular elements in the radial direction and 40 slices in the axial direction. Outside the cleft the continuous variables r and z are replaced by $r_j = j \Delta r$ and $z_k = k \Delta z$, respectively, with $0 \leq j \leq 20$, $0 \leq k \leq 40$, and $\Delta r = \Delta z = 25$ nm.

Diffusion and binding in the diadic cleft

The [Ca] inside the cleft, $U(r, t)$, satisfies the nonlinear partial differential equation (Peskoff et al., 1992; Langer and Peskoff, 1996)

$$[1 + N_1 K_1/\{h(K_1 + U)^2\} + N_2 K_2/\{h(K_2 + U)^2\}] \times \partial U/\partial t$$
$$= (D_{cleft}/r)(\partial/\partial r)(r\partial U/\partial r) + (J_{SR} + J_{chnl} + J_{xch})/h \quad (1)$$

In Eq. 1, the second and third terms in square brackets times $\partial U/\partial t$ are the number of moles of Ca per unit time per unit volume released from low- and high-affinity binding sites on the sarcolemmal surface. This is obtained by assuming that the bound Ca is in instantaneous equilibrium with the free Ca in the cleft, with the number of moles of bound Ca per unit volume given by

$$U_{bnd}(r, t) = [N_1 U/(K_1 + U) + N_2 U/(K_2 + U)]/h \quad (2)$$

where N_1 and N_2 are the number of moles of low- and high-affinity sites per unit area and K_1 and K_2 are the dissociation constants of the low- and high-affinity sites (Table 1).

D_{cleft}, the diffusion coefficient inside the cleft, is assumed to be 0.1 μm^2/ms, about one-sixth of the free aqueous diffusion coefficient (Langer and Peskoff, 1996). This reduction includes the effect of obstruction (Crank, 1975) to Ca movement by the feet of the SR, which occupy about two-thirds of the volume of the cleft.

J_{SR} is the Ca flux density into the cleft from the SR. We compute [Ca] as a function of position and time for two Ca inputs to the cleft from the SR: for a 10-ms pulse of magnitude corresponding to the SR release for near-maximum force and for an SR release of half that amount. We limit our consideration to cases where there is no azimuthal angular dependence, and assume that the spatial distribution of the Ca source is constant over the area of a 20-nm-radius circle coaxial with the sarcomere and cleft. A single Ryanodine receptor is approximately a 29×29 nm square (Radermacher et al., 1994).

The amount of Ca released to achieve near-maximum force is 2×10^{-19} per cleft for each contraction cycle (Fabiato, 1985). This amount is assumed to be released uniformly over an idealized radial cross section of 20 nm at a constant rate, starting at $t = 0$ and ending at $t = 10$ ms. In terms of current, this is 3.86 pA per cleft for 10 ms or, in terms of number of Ca ions, a total release of 125,000 ions per cleft.

The flux density for the release from the SR in Eq. 1, therefore, is

$$J_{SR}(r, t) = \begin{cases} I_{SR}/\pi q^2, & 0 \leq r \leq q \text{ and } 0 \leq t \leq \tau_{SR} \\ 0, & q < r \leq a \text{ or } t \geq \tau_{SR} \end{cases} \quad (3)$$

where $I_{SR} = 2 \times 10^{-20}$ or 1×10^{-20} moles/ms in the two examples we will consider, and $q = 20$ nm and $\tau_{SR} = 10$ ms.

J_{chnl} is the Ca flux density into the cleft from a Ca channel. We assume a 1-ms pulse corresponding to the Ca current from a single Ca channel. The radial extent of the Ca channel source is taken to be the minimum amount possible in the computation, covering the central, $i = 0$ element, which extends from the cleft center to a radius one-half of the 2.5-nm radial step size within the cleft, or 1.25 nm. This

TABLE 1 Rate constants, dissociation constants, and buffer concentrations

	k_+ (mM^{-1} ms^{-1})	k_- (ms^{-1})	K_d (mM)	Concentration (mM)
Cleft low-affinity sites*	—	—	1.1	165
Cleft high-affinity sites*	—	—	0.013	13
Calmodulin[#]	100	0.038	0.38×10^{-3}	0.024
Troponin[#]	39	0.02	0.51×10^{-3}	0.07
Fluo-3[§]	230	0.17	0.74×10^{-3}	0.1

* Post and Langer (1992). Concentration in mmoles/liter of *cleft* volume.

[#] Sipido and Wier (1991). Concentration in mmoles/liter of *sarcomere* volume.

[§] Escobar, et al. (1995). Concentration in mmoles/liter of *sarcomere* volume.

is much greater than the actual channel radius, so that the computation will yield a [Ca] much less than the actual [Ca] at distances less than 1.25 nm from the channel. The flux density for influx from the Ca channel is then

$$J_{chnl}(r, t) = \begin{cases} I_{chnl}/\pi p^2, & 0 \le r \le p \text{ and } 0 \le t \le \tau_{chnl} \\ 0, & p < r \le a \text{ or } t \ge \tau_{chnl} \end{cases} \quad (4)$$

where $I_{chnl} = 0.3$ pA, $p = 1.25$ nm, and $\tau_{chnl} = 1$ ms.

J_{xch} is the inward Ca flux density for the Na/Ca exchanger (negative for the exchanger operating in the "forward" direction with an outward Ca flux). We estimate 100 Na/Ca exchangers per cleft (Langer and Peskoff, 1996) or $N_{xch} = 100/(\pi a^2 \times \text{Avogadro's number})$ moles per unit area. We take a saturation value of $V_{xch} = 1.5$ cycles/ms. This is the value measured by Matsuoka and Hilgemann (1992), at -60 mV membrane, which is the mean transmembrane potential for a rat ventricular myocyte over a 200-ms time interval starting at the initiation of the action potential (Schanten and ter Keurs, 1985). A reversal concentration, $U_{rev} = 100$ nM, is introduced to prevent the continual extrusion of Ca from the cleft at Ca concentrations less than 100 nM. The Ca flux density through the Na/Ca exchanger is then given by

$$J_{xch}(r, t) = -N_{xch}V_{xch}(U - U_{rev})/(K_{xch} + U) \quad (5)$$

with $K_{xch} = 5\ \mu$ M (Matsuoka and Hilgemann, 1992).

Diffusion, buffering, and reuptake in the sarcomere outside the cleft

Diffusion outside the cleft occurs with a diffusion coefficient assumed to be 0.3 μm^2/ms, about half of the free aqueous diffusion coefficient (three times the coefficient assumed in the cleft). In the region of the sarcomere outside the cleft, we consider the effect of binding to fixed buffers calmodulin and troponin, using experimental values for their forward and backward rate constants and concentrations (Table 1). We also consider the effect of additional buffer, specifically the fluorescent dye fluo-3 (Minta et al., 1989; Kao et al., 1989). For simplicity, we model fluo-3 as being fixed. The effect of ignoring its mobility is to increase the computed peak [Ca] to some degree (Smith et al., 1996; Nowycky and Pinter, 1993). Completing the passage of Ca through the sarcomere, the model includes reuptake of the Ca by the longitudinal SR, assumed to be located just inside the outer cylindrical surface of the sarcomere. The diffusion equation and the three coupled kinetic equations for Ca buffering are

$$\partial C_0/\partial t = D_{sarc}[(1/r)(\partial/\partial r)(r\partial C_0/\partial r) + \partial^2 C_0/\partial z^2] + S_{cleft}$$
$$+ S_{reup} + S_{corb} - \partial C_1/\partial t - \partial C_2/\partial t - \partial C_3/\partial t \quad (6)$$

$$\partial C_1/\partial t = k_{1+}C_0(B_1 - C_1) - k_{1-}C_1 \quad (7a)$$

$$\partial C_2/\partial t = k_{2+}C_0(B_2 - C_2) - k_{2-}C_2 \quad (7b)$$

$$\partial C_3/\partial t = k_{3+}C_0(B_3 - C_3) - k_{3-}C_3 \quad (7c)$$

$C_0(r, z, t)$ is the concentration of free Ca. $D_{sarc} = 0.3$ μm^2/ms is the diffusion coefficient in the sarcomere outside the cleft. $C_1(r, z, t)$, $C_2(r, z, t)$, and $C_3(r, z, t)$ are the concentrations of Ca bound to calmodulin, troponin, and fluo-3, respectively. B_1, k_{1+}, k_{1-}, B_2, k_{2+}, k_{2-}, B_3, k_{3+}, and k_{3-} are the total concentration and forward and backward rate constants for calmodulin, troponin, and fluo-3, respectively (Table 1).

The numerical computations of [Ca] within the cleft, $U(r, t)$, and [Ca] in the sarcoplasm beyond the cleft, $C_0(r, z, t)$, are coupled in the following way: the Ca flux across the cleft boundary at $r = a$, driven by the concentration gradient just inside the cleft boundary, is the source of Ca for the sarcomere outside the cleft, and the [Ca] is continuous across $r = a$.

The Ca flux leaving the cleft at $r = a$ is $- D_{cleft}$ $(\partial U/\partial r)|_{r=a} \times 2\pi ah$. This is assumed to reappear in the sarcomere outside the cleft distributed uniformly over the volume element at $(r, z) = (a, 0)$ (extending into both halves of the sarcomere) of volume $2\pi a\ \Delta r\ \Delta z$, so that the source term in Eq. 6 from the flux exiting the cleft is

$$S_{cleft}$$
$$= \begin{cases} -D_{cleft}(\partial U/\partial r)|_{r=a}h/(\Delta r\ \Delta z), \\ \qquad a - \Delta r/2 \le r \le a + \Delta r/2, \quad -\Delta z/2 \le z \le \Delta z/2 \\ 0, \quad \text{otherwise} \end{cases}$$
$$(8)$$

The condition for continuity of [Ca] at $r = a$ is

$$C_0(a, 0, t) = U(a, t) \quad (9)$$

It is assumed that just inside the outer $r = b$ cylindrical surface of the sarcomere, reuptake of Ca by the longitudinal SR occurs such that

$$S_{reup}$$
$$= \begin{cases} -(V_{reup}/2\pi bl\Delta r)(C_0 - C_{0rev})/(K_{reup} + C_0), \\ \qquad b - \Delta r/2 \le r \le b, \quad -l \le z \le l \\ 0, \quad \text{otherwise} \end{cases}$$
$$(10)$$

The value we use for the maximum reuptake rate of the SR is $V_{reup} = 7.5 \times 10^{-21}$ moles/ms/sarcomere. The justification for this value is that it is a value which approximately balances the release and reuptake of Ca by the SR in a single contraction cycle. Also, it is essentially the same value used in the model of Luo and Rudy (1994). This is ~30 times the levels measured in vitro (Levitsky, 1981), but is probably a reasonable extrapolation to in vivo operation (MacLennon, personal communication). We use the values $C_{0rev} = 100$ nM and $K_{reup} = 1\ \mu$M in Eq. 10.

S_{corb} is the source term in Eq. 6 for release from the corbular SR (CSR). The CSR is placed on the cylindrical surface of the sarcomere an axial distance 40% of the

distance from the Z-line to the M-line (Dolber and Sommer, 1984). The axial extent of the release channel is taken to be $2\Delta z = 50$ nm, and the radial extent to be $\Delta r/2 = 12.5$ nm. In the case where we include CSR release, we assume the junctional SR (JSR) and the CSR each release half the maximum force release amount, with the CSR release occurring during the 10-ms period immediately after the JSR release period. Thus

$$S_{corb}$$

$$
= \begin{cases}
I_{SR}/(2\pi b \Delta r \Delta z), & \begin{aligned} & b - \Delta r/2 \le r \le b, \\ & 0.4\, l - \Delta z \le z \le 0.4\, l + \Delta z, \\ & \tau_{SR} \le t \le \tau_{SR} + \tau_{CSR} \end{aligned} \\
0, & \text{otherwise}
\end{cases}
$$

$$(11)$$

where $I_{SR} = 1 \times 10^{-20}$ moles/ms and $\tau_{CSR} = 10$ ms.

Boundary and initial conditions

The boundary condition at the cylindrical surface of the sarcomere is such that no Ca passes through the surface. This boundary condition assumes that the same sequence of events is occurring in adjacent sarcomeres (Isenberg et al., 1996), so that the flux to adjacent sarcomeres is balanced by the flux from them. The half-sarcomere with its cleft is considered the functional unit of the cell, which is composed of many identical units. Similarly, there is no net flux in the axial direction at the two ends (M-lines) of the sarcomere, and by symmetry between the two halves of the sarcomere on either side of the Z-line, the same is true in the axial direction at the Z-line:

$$(\partial C_0/\partial r)|_{r=b} = (\partial C_0/\partial z)|_{z=0} = (\partial C_0/\partial z)|_{z=l} = 0 \quad (12)$$

At $t = 0$ the free [Ca] everywhere is assumed to be 100 nM and the binding sites on the inner surface of the sarcolemma and the calmodulin and troponin in the sarcomere are assumed to be in equilibrium with the free Ca:

$$U(r, 0) = C_0(r, z, 0) = 100 \text{ nM} \quad (13)$$

Numerical methods

Equation 1 for [Ca] inside the cleft is solved numerically using the explicit four-point finite-difference scheme with variable forward time steps, Δt_{cleft}, described in Peskoff et al. (1992). In this numerical procedure, $U(r_i, t + \Delta t_{cleft})$ is computed from $U(r_{i-1}, t)$, $U(r_i, t)$ and $U(r_{i+1}, t)$. The boundary condition at $r = a$, which previously was $U(a, t) = 100$ nM, now is replaced by Eqs. 8 and 9. This allows $U(a, t)$ to vary to satisfy the conditions across the $r = a$ border between the cleft and the sarcomere outside the cleft. For stability of the numerical computation, the condition that we use for the size of the variable time step inside the cleft,

Δt_{cleft}, is

$$\Delta t_{cleft} \le 0.4(\Delta r_{cleft})^2 [1 + N_1 K_1/\{h(K_1 + U(0, t))^2\}$$
$$+ N_2 K_2/\{h(K_2 + U(0, t))^2\}]/D_{cleft} \quad (14)$$

where we use the value of U at $r = 0$ because it is the location where U has its maximum value for all of the centrally positioned sources that we consider. When $U(0, t) = 0.1$ μM, Eq. 14 requires $\Delta t_{cleft} \le 28$ μs. When $U(0, t) = 7$ mM, the maximum concentration we will encounter, it requires a much smaller value, $\Delta t_{cleft} \le 0.09$ μs.

The coupled Eqs. 6 and 7a, b, and c for [Ca] outside the cleft are solved numerically using a six-point explicit finite-difference scheme, with fixed forward time steps, Δt. In this numerical procedure, $C_0(r_j, z_k, t + \Delta t)$ is computed from $C_0(r_{j-1}, z_k, t)$, $C_0(r_j, z_{k-1}, t)$, $C_0(r_j, z_k, t)$, $C_0(r_j, z_{k+1}, t)$, and $C_0(r_{j+1}, z_k, t)$. For stability of this numerical procedure outside the cleft, we take

$$\Delta t = 0.2(\Delta z)^2/D_{sarc} = 0.4167 \text{ } \mu s \quad (15)$$

When Eqs. 14 and 15 yield $\Delta t_{cleft} > \Delta t$, we take $\Delta t_{cleft} = \Delta t$. This is the case for $U(0, t)$ less than ~2 mM.

The computation begins in the cleft at $t = 0$, with $U(r, 0)$ given by the initial condition of Eq. 13 and, therefore, with $\Delta t_{cleft} = \Delta t = 0.4167$ μs. The numerical solution of Eq. 1 over the first time step yields $U(r, \Delta t)$. The Ca that has diffused across the $r = a$ border during the interval $0 < t < \Delta t$ is computed from Eq. 8, using a second-order approximation of $(\partial U/\partial r)|_{r=a}$. Next, the computation of diffusion, buffering, and reuptake by the SR in the region outside the cleft (Eqs. 6, 7, and 10) is done for the interval $0 < t < \Delta t$. Finally, the Ca that diffused across the $r = a$ border during the $0 < t < \Delta t$ interval is added to the Ca in the first volume element in the region outside the cleft: $a - \Delta r/2 < r < a + \Delta r/2$, $-\Delta z/2 < z < \Delta z/2$. The [Ca] in this element, $C_0(a, 0, \Delta t)$, is adjusted to account for the added Ca, and the [Ca] on the cleft side of the $r = a$ border, $U(a, \Delta t)$, is changed so that it equals the adjusted $C_0(a, 0, \Delta t)$ (Eq. 8). The same procedure is then repeated for successive Δt intervals.

When $U(0, t)$ increases to the level for which Eqs. 14 and 15 require $\Delta t_{cleft} < \Delta t$, the computation in the cleft is done a number of times in succession until the sum of the Δt_{cleft} increments exceeds Δt. The last Δt_{cleft} increment is then adjusted downward, so that the sum of the Δt_{cleft} increments equals Δt, and the last computation inside the cleft within that Δt interval is done. During all of the Δt_{cleft} subintervals of this single Δt interval, the boundary condition at $r = a$ is kept fixed, and the cumulative Ca that has diffused across the $r = a$ border during the Δt interval is computed. Next, the computation of diffusion, buffering, and reuptake by the SR in the region outside the cleft is done for the same Δt interval; the Ca that diffused across the $r = a$ border during the Δt interval is added to the Ca in the first volume element in the region outside the cleft; $C_0(a, 0, t)$ is adjusted accordingly, and $U(a, t)$ is changed to equal the adjusted $C_0(a, 0, t)$. The same procedure is then repeated for successive Δt

intervals. When the [Ca] drops below $\sim$2 mM, the computation reverts to the procedure with $\Delta t_{cleft} = \Delta t$.

A Fortran 90 program has been written to implement this numerical procedure. The run time on a Dell Pentium Pro 200 MHz PC is $\sim$15 min for a 200-ms Ca transient.

RESULTS

Ca concentration after JSR release

For the computations illustrated in this section, Ca is assumed to be released from a single ryanodine receptor located at the center of the circular cleft. According to Eq. 3, the idealized receptor is assumed to release Ca distributed uniformly over a small circular area. This simplifying assumption is made so that the resulting Ca distribution is independent of the azimuthal angle, depending only on the radial and axial variables, r and z. Electron micrographs reveal the ryanodine receptor to be roughly square in cross section, with a side of $\sim$29 nm, separated from adjacent receptors by $\sim$7 nm (Langer and Peskoff, 1996; Wibo et al., 1991). In Eq. 3, we idealize the cross section of the receptor by a circle of radius 20 nm.

The maximum [Ca] attained inside the cleft in the immediate vicinity of the receptor increases as the radius of the receptor cross section decreases. However, some distance away at the outer boundary of the cleft, and everywhere outside the cleft, the computed concentration is found to be independent of the assumed receptor radius. For example, we have run the computation for a centrally located cluster of four receptors (40-nm radius) and nine receptors (60-nm radius). We found essentially no difference in the [Ca] outside the cleft compared to the results illustrated below for the case of a 20-nm receptor release radius, but significantly higher concentrations near the center of the cleft when the source is more concentrated. From these results, we can also expect that replacing the actual release from discrete points within an approximately square cross section, with uniform release over a circular cross section is inconsequential, except perhaps in the immediate vicinity of the receptor. In our previous paper modeling the cleft (Langer and Peskoff, 1996), we assumed that the radius of the SR release area was equal to the radius of the cleft, i.e., all ryanodine receptors in the cleft were releasing Ca simultaneously. The present assumption of a single active receptor (or perhaps several) leads to a more reasonable value of current from an individual receptor.

JSR release: 2×10^{-19} moles

Fig. 2 *A* is a graph of the free [Ca] at eight radial locations in the Z-line plane: four points inside the cleft, one point on the border between the cleft and the rest of the sarcomere outside the cleft, and three points in the sarcomere outside the cleft. These are the points shown in Fig. 1 along the radial line in the Z-line plane, from the axis to the outer radius of the sarcomere. Fig. 2 *B* shows the first 20 ms of

Fig. 2 *A*, on a 10-fold expanded time scale. Fig. 2 *C* is a three-dimensional picture of the same information as in Fig. 2 *A*, shown at 41 uniformly spaced ($\Delta t = 5$ ms) times from $t = 0$ to $t = 200$ ms and at 21 uniformly spaced ($\Delta r = 25$ nm) positions from $r = 0$ to $r = 500$ nm along the radial line in the Z-line plane. The shaded portion of the graphs represents the interior of the cleft; the unshaded portion represents the general sarcomere, outside the cleft. Note that, except for the $\Delta r = 25$ nm increments outside the cleft, the Δr and Δt increments in the graph in Fig. 2 *C* are larger than those used in the numerical computation. In the computation, $\Delta r = 2.5$ nm inside the cleft is one-tenth of the value in the graph. In the computation outside the cleft $\Delta t = 0.4167$ μs, and inside the cleft $\Delta t \leq 0.4167$ μs, which are less than 10^{-4} times the $\Delta t = 5$ ms time increments in the graph.

The graphs show that the [Ca] rises rapidly from its initial value of 0.1 μM at $t = 0$, and reaches a peak value of 7.4 mM at the center of the cleft ($r = 0$) at the end of the release period ($t = 10$ ms). After $t = 10$ ms, at which time the SR release ceases, the concentration begins to fall rapidly at the center of the cleft. Meanwhile, at the periphery of the cleft ($r = a = 200$ nm) there is a delay, and the rise begins at about $t = 3.5$ ms and reaches a peak value of 42.6 μM at $t = 10.7$ ms, followed by a more gradual fall than at the central release site. Further out radially in the general sarcomere, the delay increases somewhat and the peak concentration decreases. At the outer limit of the sarcomere ($r = b = 500$ nm), the rise begins at $\sim$4.0 ms and peaks at a concentration of 5.6 μM at $t = 11.8$ ms. The concentration everywhere returns to a value close to the initial value of 100 nM after $\sim$200 ms.

The return to 100 nM and the speed of return is governed to a large extent by four parameters in the model: the saturation rate and reversal concentration of the sodium-Ca exchanger, and the rate and reversal concentration of the SR reuptake. The saturation rate of the exchanger is an experimentally derived parameter (Matsuoka and Hilgemann, 1992). The concentration at which the exchanger reverses depends on the intra- and extracellular sodium concentrations and the membrane potential, all of which vary during the course of an action potential. We do assume, however, that reversal occurs at 100 nM and, at this point, ignore its voltage and concentration dependence. This seems a reasonable assumption at $\sim$200 ms, when the membrane potential is about -90 mV and the computed [Ca] within the cleft is approaching 100 nM. This modification in the model, compared to our earlier model (Langer and Peskoff, 1996), prevents the exchanger from continuing to extrude Ca from the cleft when it should be acting in "reverse," and thereby prevents the concentration inside the cleft from falling to unphysiological concentrations less than 100 nM.

The two reuptake parameters were selected somewhat arbitrarily to force the return to 100 nM in a time interval of $\sim$200 ms. In the absence of SR release, the reuptake must stop at some level, which we take to be 100 nM, to prevent the [Ca] from dropping to a nonphysiological level. Equa-
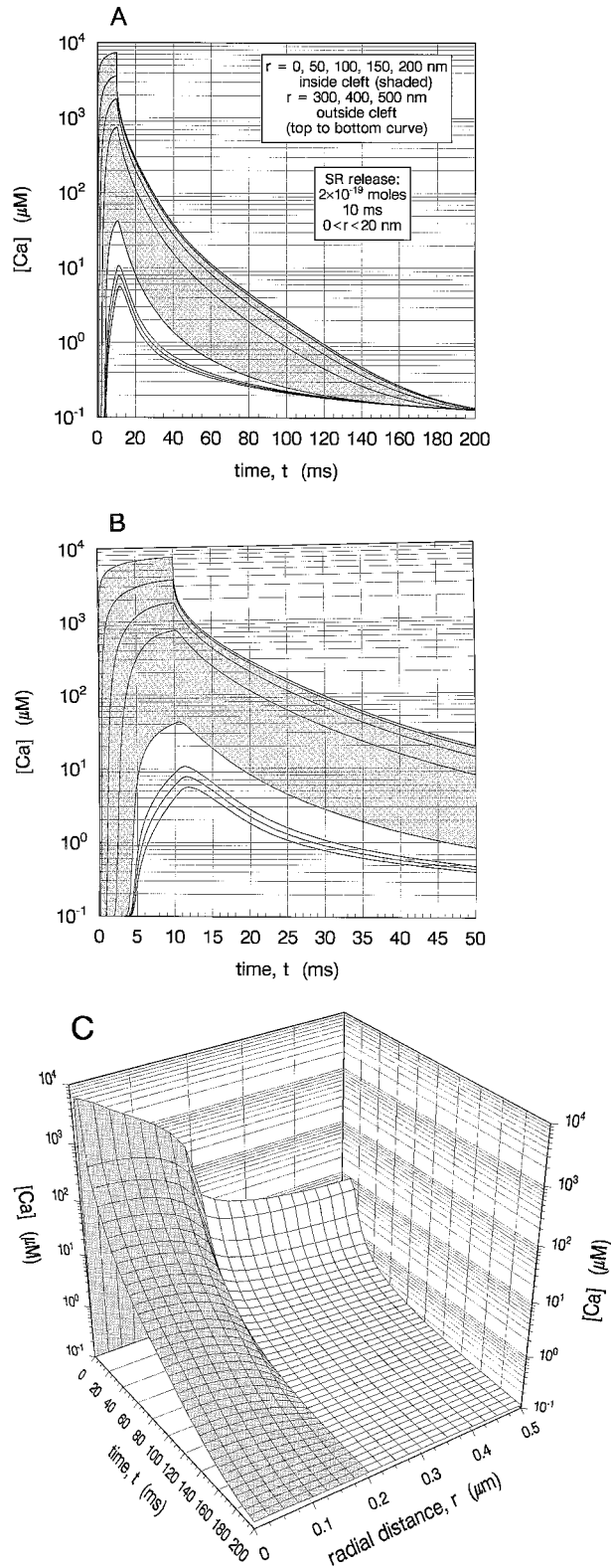
FIGURE 2   [Ca] for an SR release of 2×10^{-19} moles. (*A*) [Ca] versus *t* at the eight points in the $z = 0$ plane shown in Fig. 1. (*B*) The first 20 ms of *A* on a 10-fold expanded time scale. (*C*) Three-dimensional picture of the same information as in *A*, shown at 41 uniformly spaced times ($\Delta t = 5$ ms) and at 21 uniformly spaced positions ($\Delta r = 25$ nm) along a radial line ($0 \leq r \leq 500$ nm) in the $z = 0$ plane. The shaded portion of the graphs represents the interior of the cleft; the unshaded portion represents the sarcomere outside the cleft.

tion 10, governing the reuptake process, is obviously a simplification of the actual process, which is outside the scope of the present model, but we would not expect this simplification to have any serious impact on the computed intracellular concentrations.

Fig. 3 *A* shows graphs of the time dependence of free [Ca] at five points equally spaced between the Z-line and the M-line along a line parallel to the sarcomere axis at a distance from the axis equal to the cleft radius, shown in Fig. 1. The uppermost curve is the variation at the boundary of the cleft, and is a repeat of that curve in Fig. 2 *B* for the same point, which peaks at 43 μM. The middle solid curve at $(r, z) = (200$ nm, 500 nm$)$ is almost identical to the bottom curve in Fig. 2 *A* for $(r, z) = (500$ nm, 0 nm$)$. It reaches a peak value of 5.4 μM at $t = 12$ ms. The bottom curve in Fig. 3 *A* at $(r, z) = (200$ nm, 1000 nm$)$ at the M-line has a peak of 1.8 μM at $t = 13$ ms. Also shown, in the
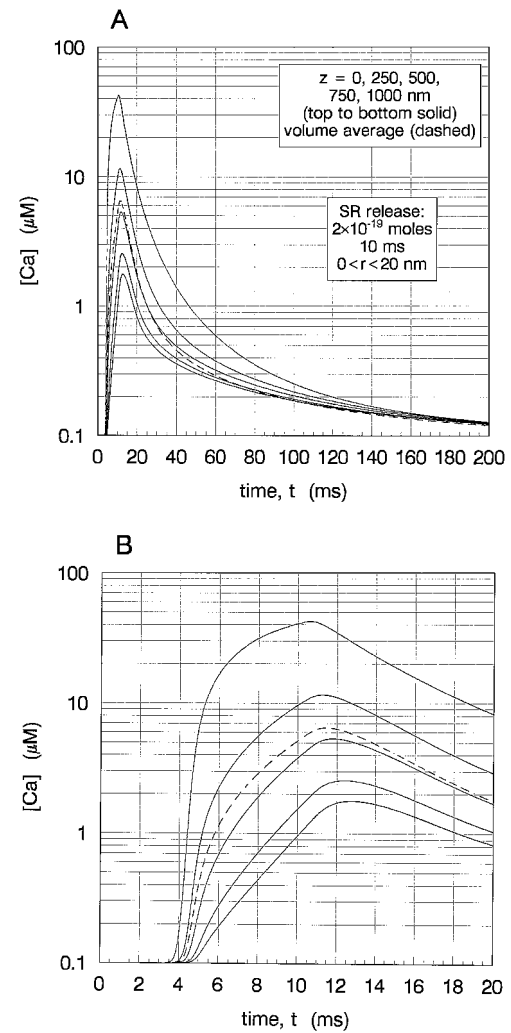

FIGURE 3   [Ca] for an SR release of 2×10^{-19} moles. (*A*) [Ca] versus *t* at the five axially spaced points at $r = a = 200$ nm shown in Fig. 1. The uppermost curve is of [Ca] at the boundary of the cleft, and is the same as the curve in Fig. 2 *B* for the same point. The dashed curve is the average of the [Ca] over the volume of the sarcomere outside the cleft. (*B*) The first 20 ms in *A* on a 10-fold expanded time scale.

dashed curve, is the average of the [Ca] over the volume of the sarcomere outside the cleft. It peaks at 6.5 μM at $t = 11.5$ ms. Thus the average concentration is approximately one-sixth of the maximum concentration that the model predicts at the boundary between the cleft and the rest of the sarcomere and indicates the magnitude of the intrasarcom-

eric Ca gradient. Fig. 3 *B* shows the first 20 ms in Fig. 3 *A* on a 10-fold expanded time scale.

Fig. 4 *A* shows four "snapshots" of the free [Ca] in the sarcomere outside the cleft at $t = 5$, 10, 20, and 50 ms, as a function of radial and axial position in the shaded plane pictured in Fig. 1. Note that the portion of the curves at

FIGURE 4 [Ca] for an SR release of 2×10^{-19} moles. (*A*) Four snapshots of the free [Ca] in the sarcomere outside the cleft at $t = 5$, 10, 20, and 50 ms, as a function of radial and axial position in the shaded plane pictured in Fig. 1. Note that the portion of the curves at $z = 0$ from $r = 0$ to $r = a = 200$ nm are of [Ca] in the Z-line plane, outside the cleft, unlike the shaded portions of Figs. 2 *A–C*, which are of [Ca] inside the cleft (see text: Geometry of the Model). (*B*) The same as in *A*, but for total [Ca] (i.e., the sum of free Ca and Ca bound to troponin and calmodulin).
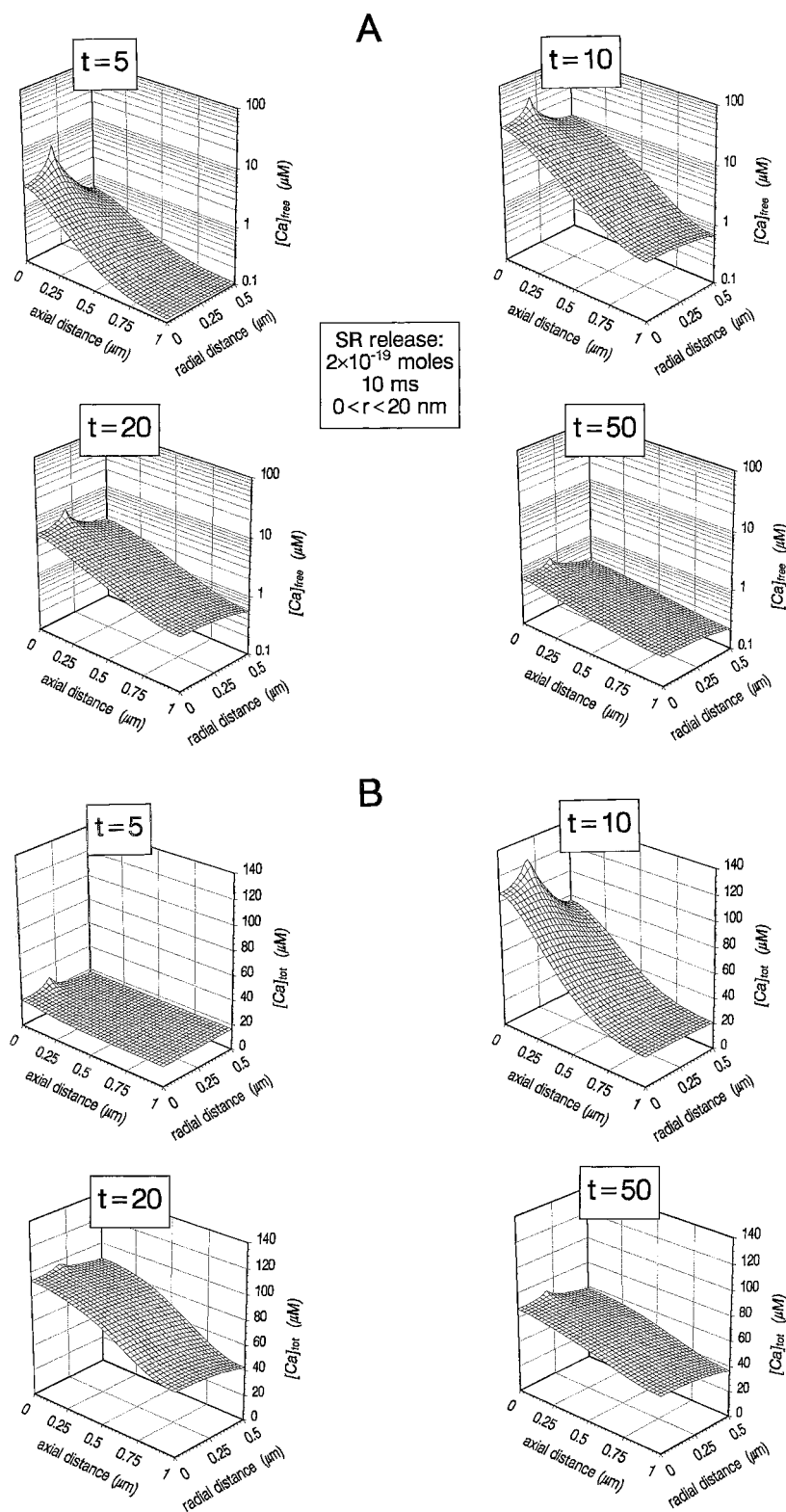
$z = 0$ from $r = 0$ to $r = 0.2$ μm are in the Z-line plane, outside the cleft, unlike the shaded portions of Fig. 2, *A–C*, from $r = 0$ to $r = 0.2$ μm, which are inside the cleft.

Again, the peak concentration is seen to occur at the boundary point between the cleft and the general sarcomere, falling off fairly rapidly in any direction away from that point, and diminishing as time progresses. At 20 and 50 ms, an approximately parabolic radial distribution has developed at the outer axial limit of the sarcomere, resulting from the Ca "sink" at the location of the SR reuptake. Fig. 4 *B*, for the same conditions as Fig. 4 *A*, shows the total [Ca] (i.e., the sum of free Ca and Ca bound to troponin and calmodulin). Note that at $t = 50$ ms, the free [Ca] ranges between 0.2 and 0.9 μM over the sarcomere, whereas total [Ca] ranges between 40 and 70 μM.

Fig. 5 *A* illustrates the partition of Ca ions among the various possible states in or departed from the cleft. The figure shows the fraction of the Ca ions, released by the SR up to the time t, that have left the cell via the exchanger, that have diffused radially out of the cleft and entered the sarcoplasm, or that are still within the cleft volume either free or bound to low- or high-affinity sites. The free and bound fractions were obtained by integrating the free and bound concentrations at time t, over the volume of the cleft; the exchanged fraction was obtained by integrating the exchanger flux density over the sarcolemmal surface of the cleft and over the time interval from 0 to t; the diffused fraction was obtained by integrating the diffusional flux density, the product of the diffusion coefficient and the radial [Ca] gradient at $r = a = 200$ nm, over the circumferential boundary of the cleft and over the time interval from 0 to t. All amounts are normalized with respect to the total SR release during the time interval 0–10 ms and multiplied by 100%.

At any instant the sum of all fractions equals the percentage of the total SR Ca that has been released up to that instant, which equals 100% after the release is over at $t = 10$ ms. At the end of the SR release ($t = 10$ ms), $\sim$55% of the Ca is bound to low-affinity sites, 9% is bound to high-affinity sites, 34% has diffused out of the cleft into the general sarcoplasm, 1% has been removed by the exchanger, and 1% is free in the cleft. At $t = 60$ ms, $\sim$91% of the Ca has diffused to the sarcoplasm, 6% has been exchanged, 2.7% is bound to the high-affinity sites, 0.6% is bound to the low-affinity sites, and 0.004% is free in the cleft. At $t = 200$ ms, 92% of the Ca has diffused to the general sarcoplasm, and 8% has been transported out through the exchanger.

In Fig. 5 *B* we have integrated over the volume of the general sarcomere outside the cleft to get the fraction of Ca ions released from the SR, up to the time t, that are free in the general sarcomere outside the cleft, that are bound to troponin or calmodulin, or that have diffused to the cylindrical boundary of the sarcoplasm, $r = 500$ nm, and have been taken up by the SR. The amounts are again normalized with respect to the total SR release. At any instant the sum
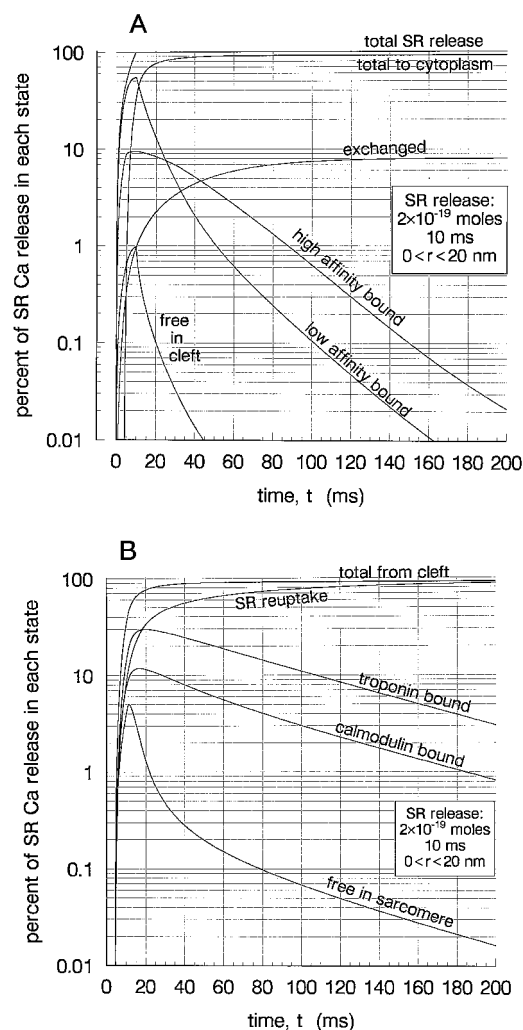

FIGURE 5   (*A*) The partition of Ca ions among the various possible states in or departed from the cleft: the fraction of the Ca ions released by the SR up to the time t that have left the cell via the Na-Ca exchanger, that have diffused radially out of the cleft and entered the sarcoplasm, or that are still within the cleft volume either free, or bound to low- or high-affinity sites. All amounts are normalized with respect to the total SR release and multiplied by 100%. Note that at $t = 200$ ms, 92% of the Ca has diffused to the general sarcoplasm and 8% has been transported out through the exchanger. (*B*) The fraction of Ca ions released from the SR up to the time t that are free in the sarcomere outside the cleft, that are bound to troponin or calmodulin, or that have diffused to the cylindrical boundary of the sarcoplasm, $r = b = 500$ nm, and have been taken up by the SR. At any instant the sum of the fractions equals the percentage of the total 10-ms-long SR release that has diffused out of the cleft up to that instant. Note that at $t = 200$ ms, $\sim$3% of the Ca is bound to troponin, 1% is bound to calmodulin, 88% has been taken up by the SR, and 0.016% is free in the sarcoplasm. The remaining 8% has exited from the cell via the Na-Ca exchanger (see *A*).

of the fractions equals the percentage of the total 10-ms-long SR release that has diffused out of the cleft up to that instant. At the end of the SR release ($t = 10$ ms), $\sim$13.9% of the released Ca is bound to troponin, 7.4% is bound to calmodulin, 8.3% has diffused to the cylindrical boundary of the sarcomere and been taken up by the SR, and 4.0% is free in the sarcoplasm. At $t = 60$ ms, $\sim$19% of the Ca is

bound to troponin, 6% is bound to calmodulin, 66% has been taken up by the SR, and 0.15% is free in the sarcoplasm. At $t = 200$ ms, ~3% of the Ca is bound to troponin, 1% is bound to calmodulin, 88% has been taken up by the SR, and 0.016% is free in the sarcoplasm. The remaining 8% has exited from the cell via the Na/Ca exchanger (see Fig. 5 *A*).

JSR release: 1×10^{-19} moles

In Figs. 6 and 7, the results for an SR release of 1×10^{-19} moles, half the amount of release in Figs. 2–5, are shown. This amount of Ca released from the SR will produce ~30% maximum force (Fabiato, 1985). Fig. 6 *A* shows that [Ca] rises to a peak value of 2.5 mM at the center of the cleft at the end of the release period. This value is less than half the value shown above for double the release because, at these concentrations, the buffering capacity of the low-affinity sites is near its saturation value. At the periphery of the cleft the rise in concentration begins after a delay of ~5 ms and reaches a peak value of 13.9 μM at 11.6 ms (compared to 3.5 ms, 42.6 μM, and 10.7 ms for an SR release of 2×10^{-19} moles). At the outer radius of the sarcomere, the rise begins at ~6 ms and peaks at ~1.0 μM at $t = 12.7$ ms (compared to 4.0 ms, 5.6 μM, and 11.8 ms).

Fig. 6 *B* illustrates the [Ca] for an SR release of 1×10^{-19} moles at five points on a line parallel to the sarcomere axis pictured in Fig. 1, and averaged over the sarcomere volume. Compared to the results for a 2×10^{-19} mole release, the peak concentrations are generally lower by somewhat more than a factor of 2, and the delay times for the start of the rise in concentration and for the occurrence of the peak are somewhat longer. Both of these effects are attributable to the greater effectiveness of the buffers at the lower concentrations.

Fig. 6 *C* shows snapshots of the free [Ca], at $t = 5, 10, 20,$ and 50 ms, as a function of radial and axial position in the shaded plane pictured in Fig. 1.

Fig. 7, showing the partition of Ca among the various states outside the cleft, is a repeat of Fig. 5 *B* for the lower SR release of 1×10^{-19} moles. It shows that at $t = 10$ ms, ~13.9% of the Ca is bound to troponin, 7.4% is bound to calmodulin, 3.7% has diffused to the cylindrical boundary of the sarcomere and been taken up by the SR, and 4.0% is free in the sarcoplasm. At $t = 60$ ms, ~19% of the Ca is bound to troponin, 7% is bound to calmodulin, 57% has been taken up by the SR, and 0.16% is free in the sarcoplasm. At $t = 200$ ms, ~4% of the Ca is bound to troponin, 1% is bound to calmodulin, 80% has been taken up by the SR, and 0.02% is free in the sarcoplasm. The remaining 15% has exited from the cell via the sodium-Ca exchanger.

SPECIAL CASES

JSR release with 100 μM fluo-3 present

The computations illustrated in this section are for conditions that are identical to those illustrated above for an SR

release of 2×10^{-19} moles, except that the fluorescent dye fluo-3 is added to the volume of the sarcoplasm outside the cleft at a 100 μM concentration.

JSR release: 2×10^{-19} moles

Fig. 8 *A* shows the free [Ca] versus time at the five axially spaced points shown in Fig. 1, for the same magnitude SR release of 2×10^{-19} moles that was present for the results shown in Figs. 2–5.

Inside the cleft (not shown) the concentration is virtually unchanged from the results shown in Fig. 2 in the absence of dye, except for a small difference close to the boundary. The concentration at the cleft boundary is shown in the uppermost curve in Fig. 8 *A*. It reaches its peak value of 36.8 μM at $t = 10.6$ ms, a short time after cessation of the JSR release, at $t = 10$ ms. In the absence of fluo-3, in Fig. 3 *A* the corresponding peak was somewhat higher (42.6 μM) and slightly later ($t = 10.7$ ms).

Away from the cleft in the sarcomere, there is a significant decrease in [Ca] resulting from the addition of 100 μM fluo-3. Comparing the bottom curves in the two figures, at the M-line the peak is reduced from just under 2 μM to just under 300 nM and is much broader, occurring after an additional delay of more than 20 ms and decaying much more slowly. However, comparing either the middle solid curves, which show the concentration midway between the Z-line and M-line, or the dashed curves, which show the concentration averaged over the volume of the sarcomere, the 100 μM fluo-3 has less but still significant effect. These show a peak reduced by a little more than a factor of 2, and broadened by about one-third. The changes in concentration, of course, are attributable to the fact that the amount of buffer has been more than doubled, from 94 μM troponin plus calmodulin to 194 μM troponin plus calmodulin plus fluo-3 (Table 1).

These results predict the extent to which, in this particular case, the use of a fluorescent dye to measure the [Ca] reduces the [Ca] that one is measuring. This is only one aspect of the problem introduced by a dye measurement. The other is the question of how accurately one can estimate free [Ca] and its time course from measurement of the amount of Ca that is bound to the fluo-3, that is, from the concentration of [Ca-fluo-3]. To investigate this, Fig. 8 *B* shows results of the computation of [Ca-fluo-3] at the five axially spaced points illustrated in Fig. 1. Comparing the volume average given by the dashed curve in Fig. 8 *B* with that in Fig. 8 *A* indicates significant differences between the time course of [Ca] and [Ca-fluo-3]. The [Ca] has a much sharper peak than the [Ca-fluo-3]. The width from half-maximum to half-maximum is ~70 ms for [Ca-fluo-3], compared to ~10 ms for [Ca]. The difference varies from a large difference between the two curves at the Z-line to two curves almost identical in shape at the M-line. This variation with location occurs because at the Z-line the [Ca-fluo-3] is at 98% saturation, whereas at the M-line it is only at 27%
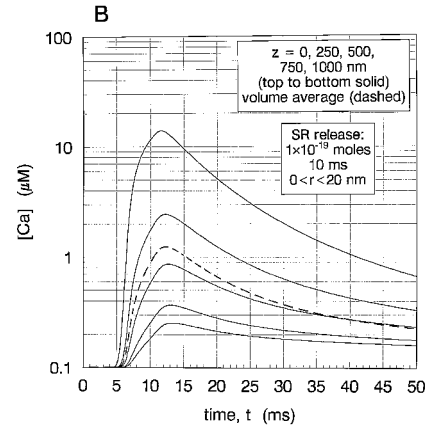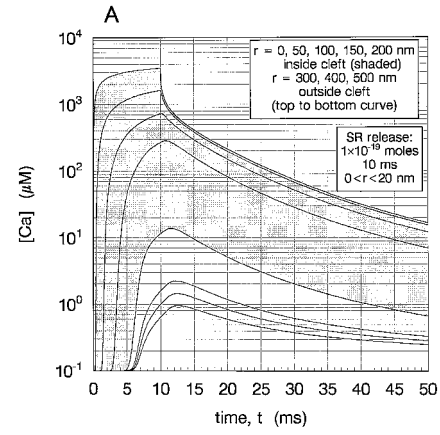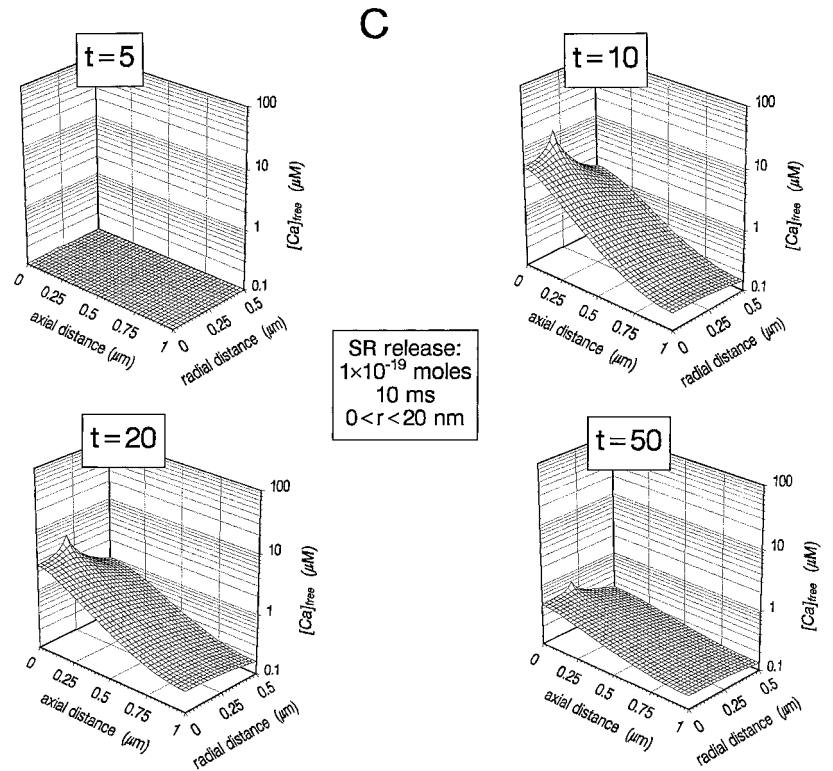
FIGURE 6 [Ca] for an SR release of 1×10^{-19} moles. (*A*) [Ca] versus *t* at the eight points in the $z = 0$ plane shown in Fig. 1. Compare to Fig. 2 *A*. (*B*) [Ca] versus *t* at the five axially spaced points at $r = a = 200$ nm, shown in Fig. 1. The dashed curve is the average of the [Ca] over the volume of the sarcomere outside the cleft. Compare to Fig. 3 *A*. (*C*) Four snapshots of the free [Ca] in the sarcomere outside the cleft at $t = 5, 10, 20,$ and 50 ms, as a function of radial and axial position in the shaded plane pictured in Fig. 1. Compare to Fig. 4 *A* for an SR release of 2×10^{-19} moles.
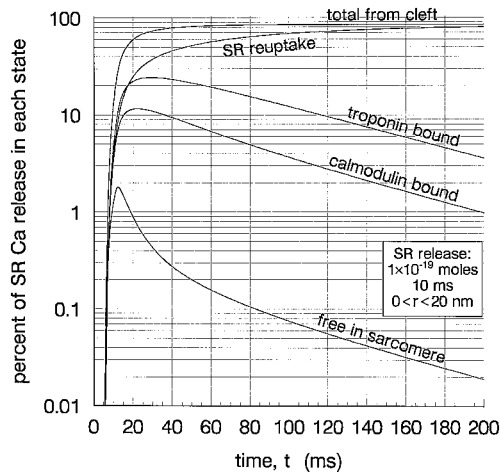
FIGURE 7   The partition of Ca among the various states outside the cleft. Same as Fig. 5 B, but for an SR release of 1×10^{-19} moles. Note that at $t = 200$ ms, ~4% of the Ca is bound to troponin, 1% is bound to calmodulin, 80% has been taken up by the SR, and 0.02% is free in the sarcoplasm. The remaining 15% has exited from the cell via the Na-Ca exchanger.

saturation and, consequently, is better able to follow the time dependence of [Ca].

Fig. 9 illustrates the partition of Ca among the various states within the volume of the sarcomere outside the cleft. The conditions are identical to those in Fig. 5 B, except for the addition of the fluo-3. At the end of the SR release ($t = 10$ ms), ~20% of the Ca is bound to fluo-3, 5.7% is bound to troponin, 3.3% is bound to calmodulin, 3.0% has been taken up by the SR, and 1.6% is free in the sarcoplasm. At $t = 60$ ms, ~16% of the Ca is bound to fluo-3, 16% is bound to troponin, 5.8% is bound to calmodulin, 52% has been taken up by the SR, and 0.2% is free in the sarcoplasm. At $t = 200$ ms, ~3.1% of the Ca is bound to fluo-3, 4.3% is bound to troponin, 1.3% is bound to calmodulin, 83% has been taken up by the SR, and 0.03% is free in the sarcoplasm. The remaining 8% has exited from the cell via the sodium-Ca exchanger, the same amount that had exited via the exchanger in the absence of fluo-3, because the fluo-3 outside the cleft has almost no influence on conditions inside the cleft.

JSR release: 1×10^{-19} moles

Fig. 10, A and B, shows the [Ca] and [Ca-fluo-3] versus time at the five axially spaced points shown in Fig. 1, for the same magnitude SR release of 1×10^{-19} moles shown in Fig. 6 B. Again, the addition of fluo-3 results in a decreased magnitude and broadened [Ca] transient and further broadening of the [Ca-fluo-3] transient.

Fig. 11 shows the partition of Ca among the various states within the sarcomere outside the cleft, averaged over the volume. It is identical to Fig. 7, except for the addition of the fluo-3, or to Fig. 9, except for the reduced SR release. At the end of the SR release ($t = 10$ ms), ~9.4% of the Ca is
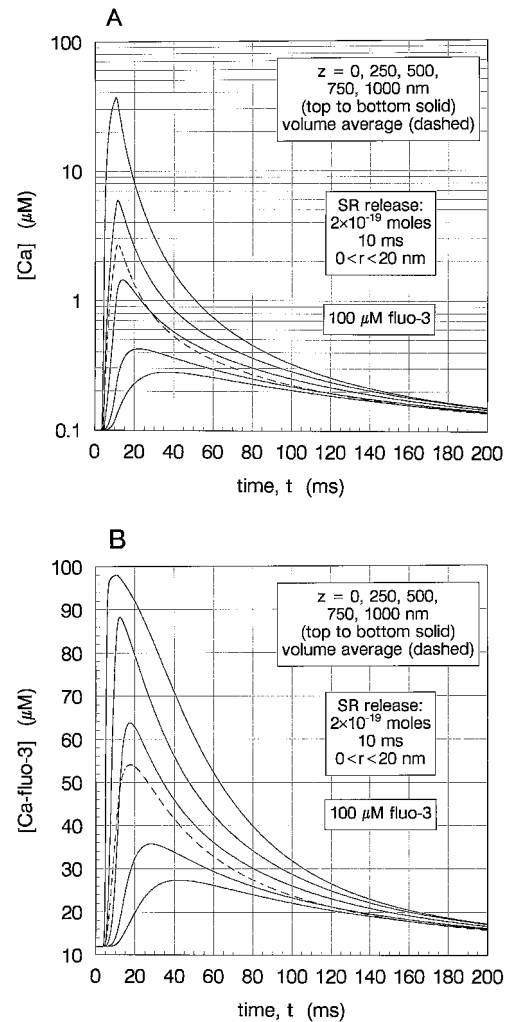

FIGURE 8   [Ca] for an SR release of 2×10^{-19} moles, with 100 μM fluo-3 added to the sarcoplasm. (A) [Ca] versus t at the five axially spaced points at $r = a = 200$ nm shown in Fig. 1. The dashed curve is the average of the [Ca] over the volume of the sarcomere outside the cleft. Compare to Fig. 3 A for the same conditions without the added fluo-3. (B) Same as in A, but for [Ca-fluo-3] and volume average of [Ca-fluo-3].

bound to fluo-3, 1.6% is bound to troponin, 1.2% is bound to calmodulin, 0.8% has diffused to the cylindrical boundary of the sarcomere and been taken up by the SR, and 0.5% is free in the sarcoplasm. At $t = 60$ ms, ~18% of the Ca is bound to fluo-3, 17% is bound to troponin, 7% is bound to calmodulin, 41% has been taken up by the SR, and 0.19% is free in the sarcoplasm. At $t = 200$ ms, ~3.6% of the Ca is bound to fluo-3, 5.0% is bound to troponin, 1.6% is bound to calmodulin, 75% has been taken up by the SR, and 0.03% is free in the sarcoplasm. The remaining 15% has exited from the cell via the sodium-Ca exchanger.

[Ca] after entry from the Ca channel

In the computations illustrated in this section, Ca is assumed to enter via a single L-type Ca channel located at the center of the cleft. The channel injects a 1-ms, 0.3 pA rectangular
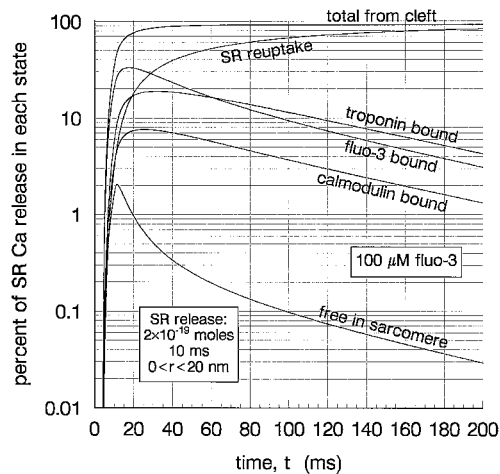
FIGURE 9   The partition of Ca among the various states outside the cleft. Same as Figs. 5 *B* and 7, but for an SR release of 2×10^{-19} moles, with 100 μM fluo-3 added to the sarcoplasm. Note that at $t = 200$ ms, ~3.1% of the Ca is bound to fluo-3, 4.3% is bound to troponin, 1.3% is bound to calmodulin, 83% has been taken up by the SR, and 0.03% is free in the sarcoplasm.

pulse (~1000 ions). The Ca flux is distributed uniformly over the area covered by the central, $i = 0$, radial element in the computation. It extends from the cleft center at $r = 0$, to a circle of radius $r = 1.25$ nm, which is one-half a radial increment ($\Delta r = 2.5$ nm) from the center. Because the actual channel radius is smaller than 1.25 nm, the computation does not resolve the peak concentration that the diffusion equation would predict for $r < 1.25$ nm for the more localized channel source. Compared to the ryanodine channel release pulse, the amplitude and duration of the current for the Ca channel are each an order of magnitude smaller, and the flux entry area is more than two orders of magnitude smaller.

In our previous paper, which modeled only the interior of the cleft (Langer and Peskoff, 1996), we presented a computation that was stated to be for an identical 0.3-pA Ca channel source. The results presented there were actually for a source of 2.7 pA rather than for the stated 0.3 pA. Consequently, the present results inside the cleft predict smaller Ca concentrations than in the previous paper by a factor of almost 10.

Fig. 12 is a graph of the free [Ca] versus time, over the range $0 \leq t \leq 20$ ms, at nine radial distances from the cleft center to the outer radius: $r = 0$, 25, 50, 75, 100, 125, 150, 175, and 200 nm. The $r = 0$ curve, which represents the mean concentration over a circle of 1.25 nm radius, has a peak concentration of 0.94 mM. At a distance of $r = 25$ nm from the center of the channel, [Ca] rises to a peak 83 μM at the end of the Ca influx at $t = 1$ ms and then declines fairly rapidly after the channel closes. At $r = 50$ nm the rise in [Ca] begins at about $t = 0.5$ ms after the channel opens, reaches a peak of 12 μM at $t = 2$ ms and then declines more gradually than the $r = 25$ nm curve. The $r = 200$ nm curve rises only a small amount above 100 nM. It is still rising at
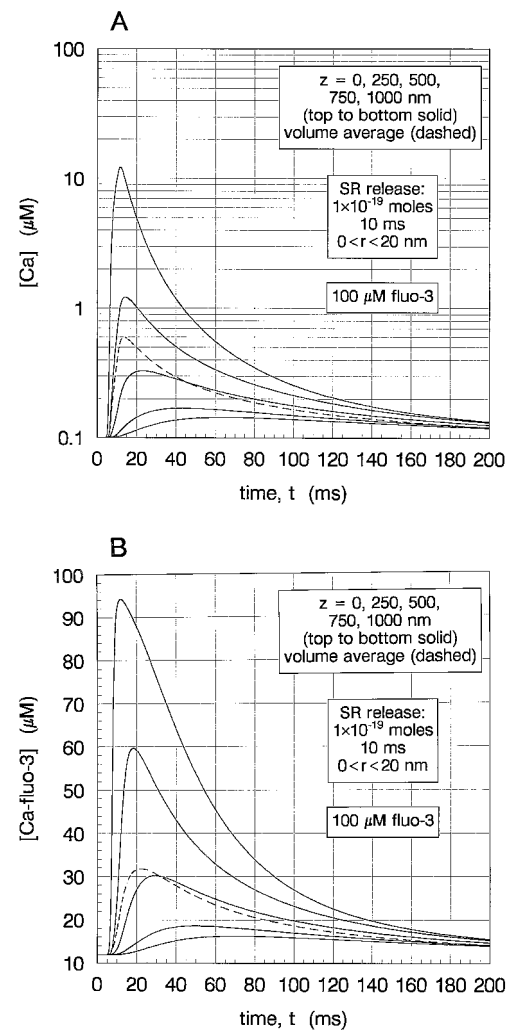

FIGURE 10   Same as in Fig. 8, but for an SR release of 1×10^{-19} moles, with 100 μM fluo-3 added to the sarcoplasm. (*A*) [Ca] versus *t* at the five axially spaced points at $r = a = 200$ nm, shown in Fig. 1. The dashed curve is the average of the [Ca] over the volume of the sarcomere outside the cleft. Compare to Fig. 6 *B* for the same conditions without the added fluo-3. (*B*) Same as in *A*, but for [Ca-fluo-3] and volume average of [Ca-fluo-3].

$t = 20$ ms and reaches a peak of 111 nM at about $t = 30$ ms (not shown). Fig. 13 is a snapshot of [Ca] on the shaded plane in Fig. 1 at $t = 30$ ms. It indicates that the release from a single Ca channel has a trivial effect on [Ca] outside the cleft.

Ca spark

The increase in free [Ca] in the sarcomere calculated above for near maximum-force release from the SR is much too large to be classified as a Ca spark, whereas the increase calculated for Ca entry from a single L-type Ca channel is much too small. In this section we present an example of release of an amount of Ca from the SR which is intermediate between these two extremes, for which the predicted increase in [Ca] is in the range of a Ca spark (Cheng et al., 1993; Santana et al., 1996).
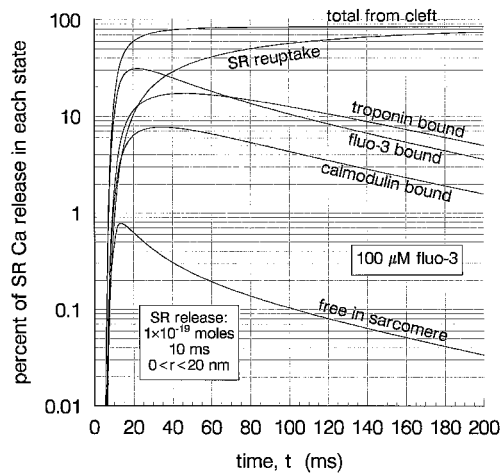
FIGURE 11   The partition of Ca among the various states outside the cleft. Same as in Figs. 5 *B* and 9, but for an SR release of 1×10^{-19} moles, with 100 μM fluo-3 added to the sarcoplasm. Note that at $t = 200$ ms, ~3.6% of the Ca is bound to fluo-3, 5.0% is bound to troponin, 1.6% is bound to calmodulin, 75% has been taken up by the SR, and 0.03% is free in the sarcoplasm. The remaining 15% has exited from the cell via the Na-Ca exchanger.

Fig. 14, *A* and *B*, shows the free [Ca] at the points illustrated in Fig. 1: at eight radial distances in the Z-line plane inside and outside the cleft, and at five axial distances from the Z-line plane in the sarcomere at a radial distance equal to the cleft radius and averaged over the sarcomere volume, respectively. Fig. 14 *C* is a snapshot at $t = 8$ ms, the instant of peak [Ca] outside the cleft, on the shaded plane in Fig. 1. The superimposed heavy curves are constant [Ca] contours: [Ca] = 0.2, 0.5, 1.0, and 2.0 μM. The rate of
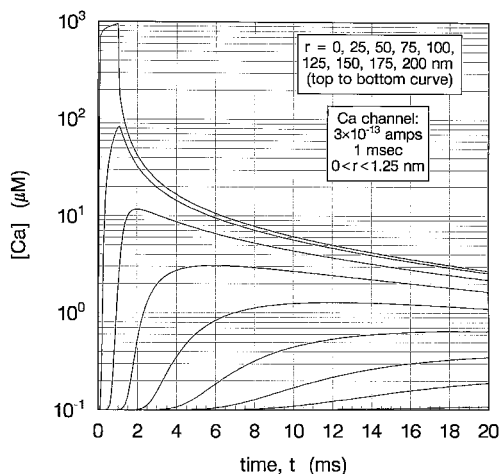

FIGURE 12   Free [Ca] versus *t* at nine radial distances from the cleft center, $r = 0$, to the cleft outer radius, $r = a = 200$ nm after 1 ms of L-channel opening. The $r = 0$ curve, which represents the mean concentration over a circle of 1.25 nm radius, has a peak concentration of 0.94 mM. The $r = 200$ nm curve rises only a small amount above 100 nM, is still rising at $t = 20$ ms, and reaches a peak of 111 nM at about $t = 30$ ms (not shown).
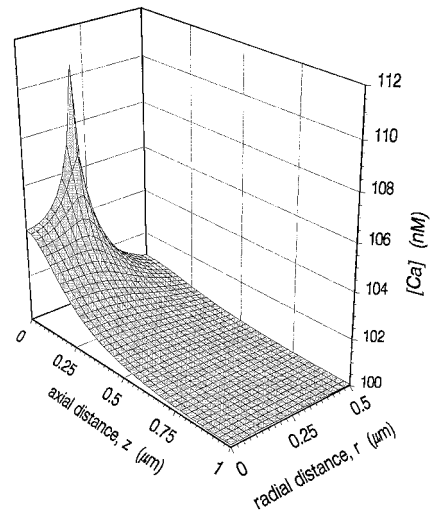

FIGURE 13   Snapshot of [Ca] on the shaded plane in Fig. 1. at $t = 30$ ms after channel opening, the time at which [Ca] at $r = a = 200$ nm reaches its maximum value. It indicates that the release from a single Ca channel at the center of the cleft has a trivial effect on [Ca] outside the cleft.

release in this example is 2×10^{-20} moles/ms/cleft, the same rate as for the maximum-force case considered above, but the duration is only 2 ms (i.e., for a total release which is one-fifth of the maximum-force release or ~26 times the amount of Ca entering through the L-type channel).

At the center of the cleft there is a rapid rise to [Ca] > 5 mM at $t = 2$ ms. At the outer radius of the cleft [Ca] is unchanged for almost 4 ms, then rises to [Ca] > 3 μM at $t = 8$ ms (Fig. 14 *A*). Away from the cleft in the sarcomere there is an additional delay of from a fraction of a millisecond to the beginning of the rise, to several milliseconds to the peaks, and the peaks decrease in magnitude as *r* or *z* increases (Fig. 14, *A* and *B*). At $t = 8$ ms, the instant when [Ca] at the $r = a = 200$ nm exit of the cleft is at its peak value, [Ca] decreases to ~1 μM within 125 nm of the exit in the axial direction or within about 50 nm in the radial direction (1 μM contour in Fig. 14 *C*). The concentration averaged over the volume has a peak value of 300 nM (Fig. 14 *B*). Note that the first 2-ms period of Fig. 14 *A* is identical to the first 2-ms period of Fig. 2, *A* and *B*.

Fig. 15 illustrates the effect of adding 100 μM fluo-3 to the sarcoplasm. Inside the cleft the effect is negligible, but outside it is significant: the peak concentrations are lower and the peaks are delayed and broadened. For example, comparing Fig. 14, *A* and *B*, with Fig. 15, *A* and *B*, at $(r, z) = (300$ nm, 0 nm$)$ or $(200$ nm, 250 nm$)$, the peak [Ca] is reduced from 500 nM to 300 nM, the time to peak has an additional delay of ~10 ms, and the decay following the peak is much slower. The peak in the volume averaged [Ca] is reduced from 300 nM to < 200 nM, delayed by an additional 5 ms and after the peak falls off much more slowly. Comparing the curves in Fig. 15 *B* (free Ca) with the curves in Fig. 15 *C* (Ca bound to fluo-3) indicates that there is an additional delay and broadening of the peaks for [Ca-fluo-3] transients compared to those for [Ca]. Compar-
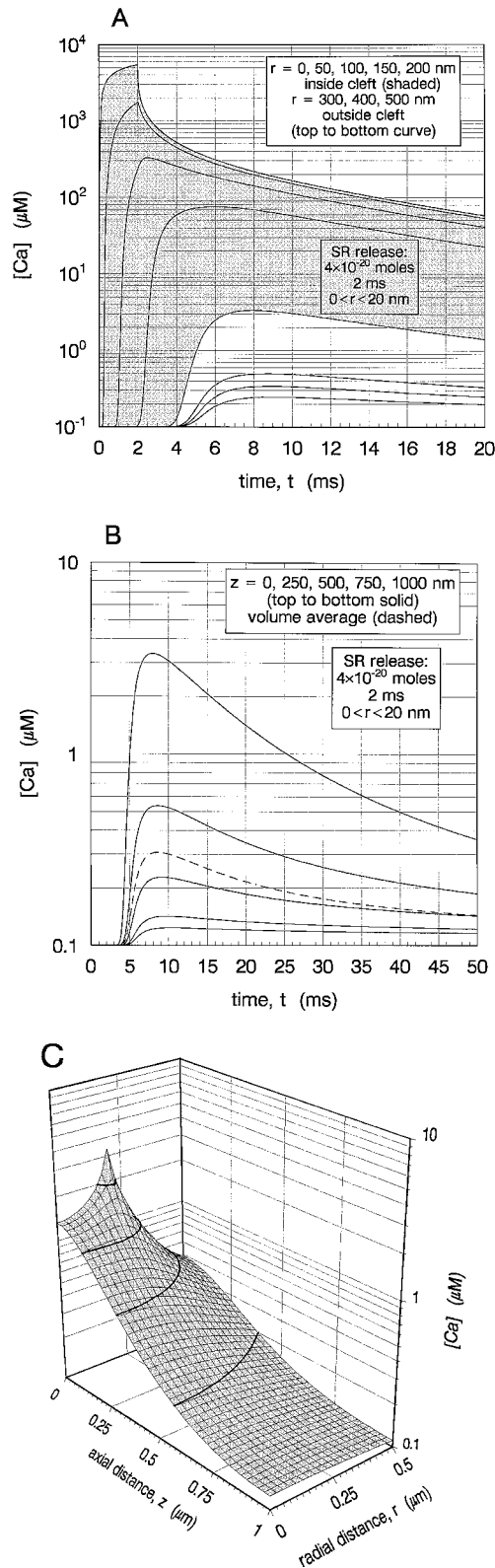
A

r = 0, 50, 100, 150, 200 nm
inside cleft (shaded)
r = 300, 400, 500 nm
outside cleft
(top to bottom curve)

SR release:
4×10^{-20} moles
2 ms
$0 < r < 20$ nm

B

z = 0, 250, 500, 750, 1000 nm
(top to bottom solid)
volume average (dashed)

SR release:
4×10^{-20} moles
2 ms
$0 < r < 20$ nm

C

FIGURE 14   [Ca] for an SR release of 4×10^{-20} moles in a 2-ms-duration pulse. A release of this magnitude simulates a Ca spark. (*A*) [Ca] versus t at the eight radially spaced points in the $z = 0$ plane, shown in Fig. 1. (*B*) [Ca] versus t at the five axially spaced points at $r = a = 200$ nm, shown in Fig. 1. The dashed curve is the average of the [Ca] over the volume of the sarcomere outside the cleft. (*C*) Snapshot at $t = 8$ ms, the instant of peak [Ca] outside the cleft, on the shaded plane in Fig. 1. The

ing the snapshots at $t = 8$ ms in Figs. 15 *D* and 14 *C* indicates that the [Ca] transient is more localized spatially when 100 μM fluo-3 is present. For example, the 500 nM contour in Fig. 15 *D* and the 1 μM contour in Fig. 14 *C* are at about the same distance from the cleft exit.

Secondary Ca release from the corbular SR

In this section we investigate the response to a release of Ca into the cleft from the JSR followed by a release into the sarcomere outside the cleft from the corbular SR (CSR). We assume a 1×10^{-19} mole release at the center of the cleft, identical to the second example considered above, i.e., of 10 ms duration over the area of a circle of 20-nm radius. In addition, we assume a delayed secondary release of the same magnitude and duration from the CSR. The CSR source is assumed to be located on a ring at $r = 500$ nm, on the outer surface of the sarcomere, extending axially from $z = 375$ to 425 nm. This is accomplished in the numerical computation by placing one 0.5×10^{-19} mole source at $(j, k) = (20, 16)$ and two 0.25×10^{-19} mole sources at $(j, k) = (20, 15)$ and (20, 17), where j and k are the radial and axial indexes in the computation: $j = r_j/\Delta r$, $0 \le j \le 20$, $\Delta r = 25$ nm; $k = z_k/\Delta z$, $0 \le k \le 40$, $\Delta z = 25$ nm.

The CSR source is assumed to be active during the period $10 \le t \le 20$ ms. Consequently, the results shown in Fig. 6 for the 1×10^{-19} mole source are valid for the present case until the instant $t = 10$ ms, when the CSR source begins to release Ca. According to the 10 ms snapshot shown in Fig. 6 *C*, at $(r, z, t) = (500$ nm, 400 nm, 10 ms) the [Ca] is ~0.5 μM. This then is the [Ca] at the location of the CSR just before the time of the initiation of Ca release from the CSR. Thus, starting the CSR release at $t = 10$ ms is equivalent to assuming that 0.5 μM is the trigger [Ca] that induces Ca release from the CSR.

Fig. 16 shows [Ca] versus time in the Z-line plane at four radial distances inside the cleft, at the radius of the cleft boundary and at three radial distances outside the cleft. The first 10 ms are identical to the results shown in Fig. 6 *A* for a release of 1×10^{-19} moles inside the cleft. After 10 ms there is an additional surge in [Ca] outside the cleft, but inside the cleft [Ca] is relatively unaffected. Comparing Fig. 16 with Fig. 2 *A*, where the same total of 2×10^{-19} moles was released during a 10 ms period, but entirely inside the cleft, indicates that dividing the release between JSR and CSR over a total 20 ms duration yields somewhat lower peak values, but more sustained increases in [Ca]. Fig. 17 shows snapshots of [Ca] versus position in the shaded plane pictured in Fig. 1, at four instants after initiation of the CSR release: $t = 15$, 20, 25, and 50 ms. The snapshots before

superimposed heavy curves are constant [Ca] contours: [Ca] = 0.2, 0.5, 1.0, and 2.0 μM (*bottom to top*). The rate of release in this example is 2×10^{-20} moles/ms/cleft, the same rate as for the maximum-force case considered above, but the duration is only one-fifth as long.
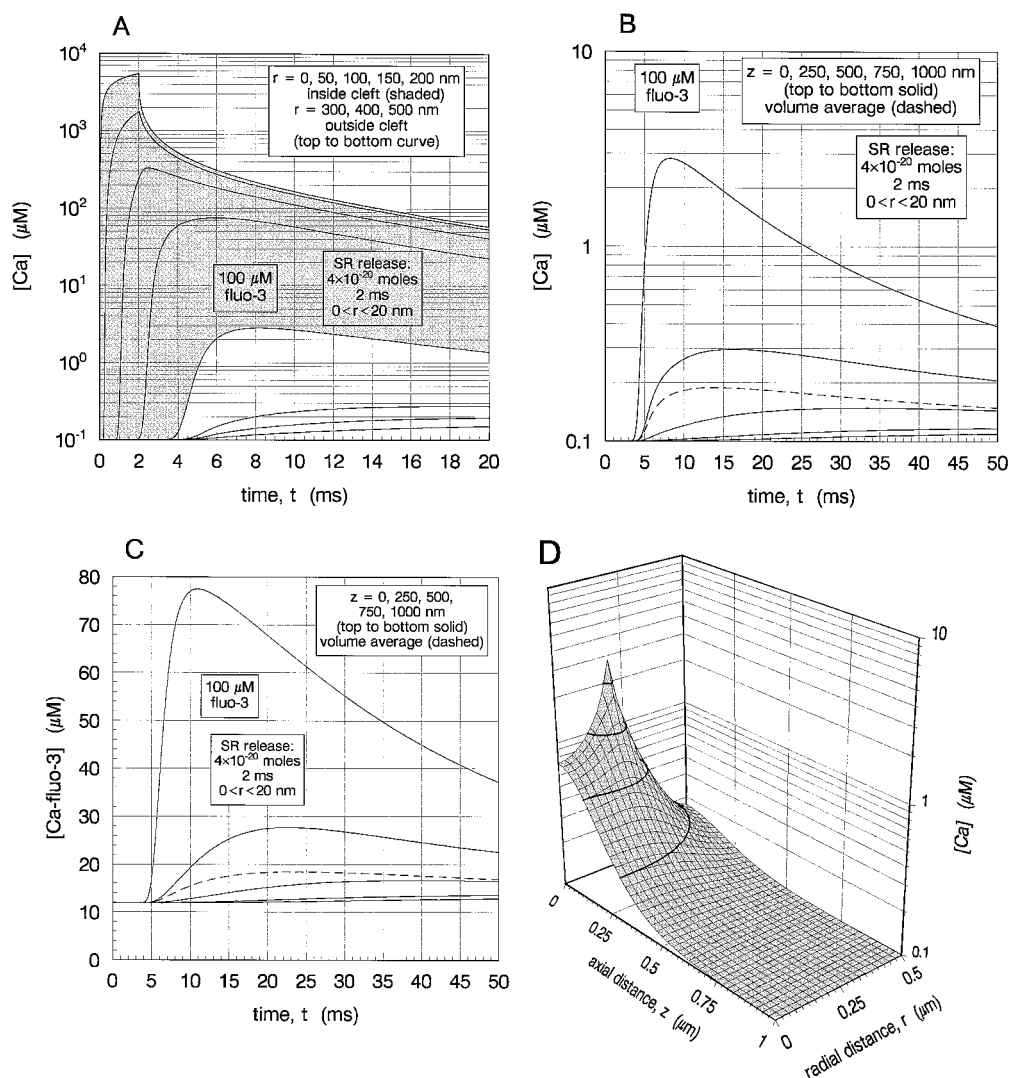
FIGURE 15 Same SR release of 4×10^{-20} moles in a 2-ms-duration pulse, as in Fig. 14, but with the addition of 100 μM fluo-3 to the sarcoplasm. (*A*) [Ca] versus *t* at the eight radially spaced points in the *z* = 0 plane, shown in Fig. 1. (*B*) [Ca] versus *t* at the five axially spaced points at *r* = *a* = 200 nm, shown in Fig. 1. The dashed curves are the average of the [Ca] over the volume of the sarcomere outside the cleft. (*C*) Same as in *B*, but for [Ca-fluo-3] and volume average of [Ca-fluo-3]. (*D*) Snapshot at *t* = 8 ms, the instant of peak [Ca] outside the cleft, on the shaded plane in Fig. 1. The superimposed heavy curves are constant [Ca] contours. Comparing Figs. 14 *A* and *B* with 15 *A* and *B*, inside the cleft the effect of adding fluo-3 is negligible, but outside it is significant: the peak concentrations are lower and the peaks are delayed and broadened. Comparing Fig. 15 *B* ([Ca]) with Fig. 15 *C* ([Ca-fluo-3]) indicates an additional delay and broadening of the peaks for [Ca-fluo-3] transients compared to those for [Ca]. Comparing Figs. 15 *D* and 14 *C* indicates that the [Ca] transient is more localized spatially when 100 μM fluo-3 is present.

CSR release for *t* = 5 and 10 ms are shown in Fig. 6 *C*. The effect of the CSR release is to form a second peak at the CSR release ring, and a plateau region between this peak and the peak at the cleft exit during the period 10 < *t* ≤ 20 ms. Note that the CSR peak disappears rapidly. The cleft peak persists because the movement of Ca from the cleft into the rest of the sarcomere, slowed by retention by the cleft binding sites, is slower than the square pulse entry from the CSR. The *t* = 20 ms snapshot in Fig. 4 *A* does not have the plateau that is present in the *t* = 20 ms snapshot in Fig. 17. At *t* = 50 ms, the snapshot is almost the same as the *t* = 50 ms snapshot for a total 2×10^{-19} mole release inside the cleft shown in Fig. 4 *A*.

DISCUSSION

Figs. 2–5 show the results for a release of 2×10^{-19} moles of Ca from a single ryanodine receptor (RyR) located at the center of the diadic cleft. This is the amount necessary to achieve maximum force (Fabiato, 1985). We have modeled the case in which it is for 10 ms at a constant rate of 2×10^{-20} moles/ms, or 3.86 pA. Experimental measurements of current and open times for single RyR range from <1 to 4 pA and from <5 to 20 ms (Rousseau et al., 1986; Rousseau and Meissner, 1989). Our assumption is for this range, but we could equally well have assumed, for example, eight RyRs, each conducting 1 pA for 5 ms. In our earlier papers
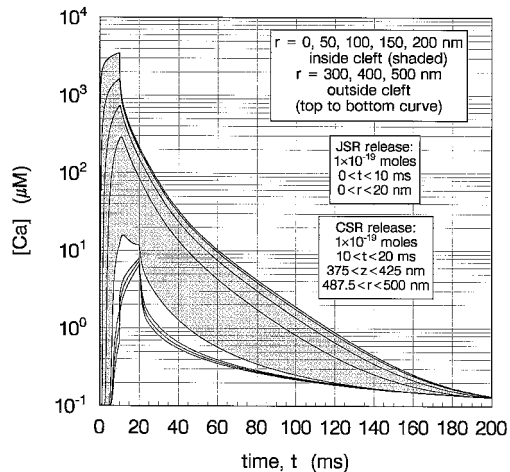
FIGURE 16   [Ca] versus t at the eight radially spaced points in the $z = 0$ plane, shown in Fig. 1. 1×10^{-19} moles of Ca is released into the cleft from the JSR between $t = 0$ and $t = 10$ ms, followed by an equal release into the sarcomere outside the cleft from the CSR between $t = 10$ and $t = 20$ ms. The first 10 ms are identical to the results shown in Fig. 6 A for a release of 1×10^{-19} moles inside the cleft. After 10 ms there is an additional surge in [Ca] outside the cleft, but inside the cleft [Ca] is relatively unaffected. Comparing Fig. 16 with Fig. 2 A, where the same total of 2×10^{-19} moles was released during a 10-ms period, but entirely inside the cleft, indicates that dividing the release between JSR and CSR over a total 20 ms duration yields somewhat lower peak values, but more sustained increases in [Ca].

(Peskoff et al., 1992; Langer and Peskoff, 1996), we considered the case when all (~100) of the RyRs in the cleft were conducting simultaneously for 20 ms. In this case each individual RyR is conducting 0.02 pA, which seems too low. The results of our present computations indicate, however, that outside the cleft (but not inside) the response is very insensitive to which assumption is made for the distribution of active RyRs. This is helpful if one wants to predict Ca distribution in the sarcomere outside the cleft with limited knowledge about the form of the RyR release, but is a disadvantage if one wants to do the inverse (i.e., infer the distribution of open RyRs from experimental measurements of Ca distribution outside the cleft).

Fig. 2 shows the [Ca] distribution versus r and t at $z = 0$ (at the Z-line). It illustrates a drop in concentration between the release location, inside a 20-nm-radius circle centered at $r = 0$ within the cleft, and the re-uptake location, on the outer cylindrical surface of the sarcomere at $r = 500$ nm. At the time of termination of the SR release, at the center of the cleft, [Ca] reaches a peak of over 7 mM. After a slight delay, at the outer boundary of the cleft [Ca] reaches over 40 μM and at the outer radius of the sarcomere it reaches > 5 μM.

The peak reached at the center of the cleft depends on the spatial and temporal extent of the Ca source. In the case considered earlier (Langer and Peskoff, 1996) where the release was over a 20 ms period, distributed uniformly over the cleft, with the cleft boundary fixed at 100 nM, the peak [Ca] at the center of the cleft was 600 μM.

The gradient is steeper inside the cleft (shaded in Fig. 2) than it is in the general sarcoplasm outside the cleft. This is

a consequence of two factors in the model: first, the diffusion coefficient inside the cleft is one-third as large as in the general sarcoplasm and second, there is a greater concentration of binding sites in the cleft than in the general sarcoplasm (Table 1), which further retards the movement of the Ca. The steepest gradient across the cleft occurs immediately following termination of the SR release ($t = 10$ ms), just inside the boundary of the cleft ($r = 200$ nm). For the most part, the concentration falls monotonically with increasing radius. Because there is also a Ca sink inside the cleft (the Na/Ca exchanger) eventually, when sufficient time has passed after the SR release is turned off, a small gradient in the opposite direction develops and the concentration has its maximum value at some point other than $r = 0$. The development of this, with a maximum at $r = 200$ nm, is beginning but barely perceptible in Fig. 2 C at $t = 200$ ms.

Fig. 3 shows a correspondingly larger variation of [Ca] along the longer dimension in the axial direction: from the 40 μM peak at the exit of the cleft in the plane of the Z-line at $t \approx 11$ ms, to a 2 μM peak at the M-line at $t \approx 13$ ms and a 6 μM peak in the [Ca] averaged over the volume of the sarcomere at $t \approx 12$ ms. This is also evident in the $t = 10$ ms snapshot in Fig. 4 A. The $t = 10$ ms snapshot of total (free + bound) [Ca] shown in Fig. 4 B indicates that at the cleft exit about one-third of the Ca is free and two-thirds is bound to calmodulin and troponin, while at the M-line only about one-thirtieth of the Ca is free, and that the axial gradient of free [Ca] is much larger than the axial gradient of bound [Ca]. The magnitude of the intrasarcomeric gradients is striking. Shortly following end-release the model predicts a gradient of > 3 orders of magnitude from cleft center to M-line. Fifty milliseconds after release this gradient is still >30 fold. Outside the cleft the axial gradient is >3 from Z to M-line at 40 ms after cessation of release. There is a delay of 4–5 ms before [Ca] begins to rise outside the cleft whereupon it rises most rapidly for the next 8–10 ms (Figs. 3 B and 6 B). This pattern almost exactly predicts the sequence found by Isenberg et al., (1996) using Ca indicators and high speed three-dimensional digital imaging microscopy.

The [Ca] snapshots (Fig. 4) depict the simultaneous radial and axial sarcomeric gradients of 5, 10, 20, and 50 ms after initiation of SR Ca release. These indicate steep gradients at early times (5, 10 ms) which then decline over the next 40 ms (Fig. 4 A). Similar plots made by Wier and Yue (1986) show very similar results. Ca binding gradients (Fig. 4 B) initially lag behind free [Ca] gradients but as binding sites approach saturation ($t = 10$ and 20 ms) they tend to parallel the free gradients and become "flatter" at 50 ms. As the [Ca] transient forms and spreads the sarcomeric distribution of Ca is plotted in Figs. 5 A (for the various states in and departed from the cleft) and 5 B (for the various states in and departed from the remainder of sarcomere).

In the cleft note that 1) At peak [Ca]$_{\text{free}}$ of 7 mM in the cleft at 10 ms (Fig. 2 A) the free Ca represents only 1% of the total released by the SR. 2) At end release (10 ms)

FIGURE 17 Snapshots of [Ca] versus position in the shaded plane pictured in Fig. 1, at four instants after initiation of the CSR release: t = 15, 20, 25, and 50 ms. The snapshots before CSR release for t = 5 and 10 ms are shown in Fig. 6 *C*. The effect of the CSR release is to form a second peak at the CSR release ring, and a plateau region between this peak and the peak at the cleft exit during the period $10 < t \leq 20$ ms. The CSR peak disappears rapidly but the cleft peak persists because the movement of Ca out of the cleft is slower than the 10 ms duration of the Ca pulse entering from the CSR.
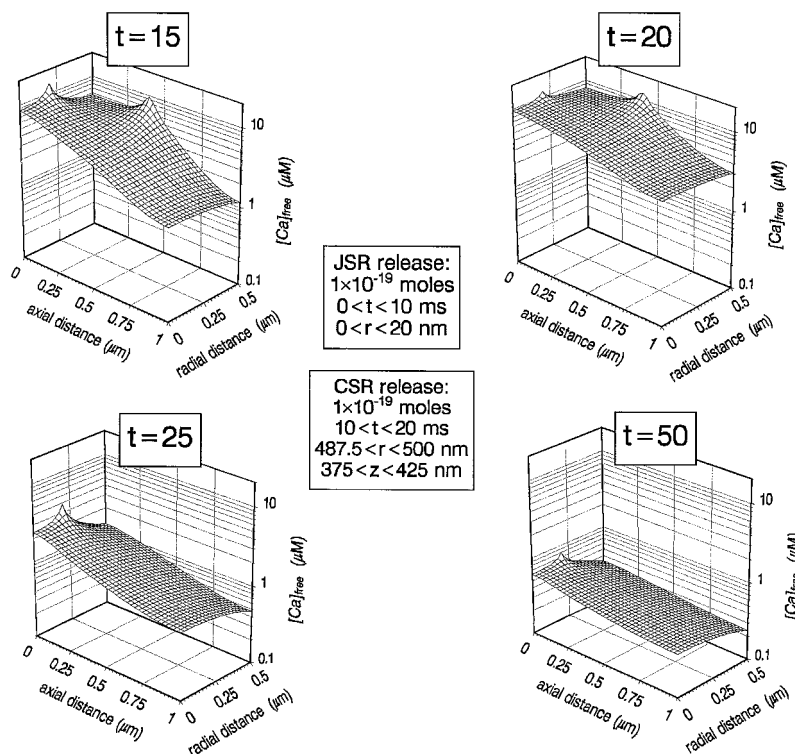
>50% of the total is bound to low affinity inner sarcolemmal phospholipid binding sites (Post and Langer, 1992). 3) At 30 ms, when virtually all release to the cytoplasm has taken place and [Ca] free in the cleft represents 0.03% of the total released, 11% of the release is still bound to the low and high affinity sites. It is this Ca that provides the bulk of Ca destined to leave the cell via Na/Ca exchange during the next 100 msec (see curve designated "exchanged" in Fig. 5 *A*). 4) About 8% of release exits via Na/Ca exchange when the release is high. This fraction is similar to that found by Bassani et al. (1994).

In the sarcomere (Fig. 5 *B*) note that: 1) There is about a 5-ms delay after SR release before sarcoplasmic Ca begins to rise. Isenberg et al., (1996) measured a similar delay and ascribed it to slow activation of dihydropyridine sensitive Ca channels. The model indicates that the delay is most likely due to diffusional delay within the cleft. 2) [Ca]$_{free}$ reaches its maximum level at ~12 ms, and this agrees with recent results obtained by high-speed digital imaging microscopy (Isenberg et al., 1996). One would also predict that maximum rate of force development would be achieved within this period of time and this has been shown to be the case (Spurgeon et al., 1990). 3) After 60 ms the rates of decline of free [Ca], troponin bound Ca and calmodulin bound Ca are the same. This indicates an equilibrium among these three components after SR reuptake is ~80% complete.

It should be noted that the greater variation seen in the axial direction than in the transverse direction occurs simply because the axis of the half-sarcomere is longer than its radius, not because the [Ca] gradients in the two orthogonal directions differ greatly in magnitude. This, of course,

would change if we assumed that the sarcoplasm was an anisotropic medium with differing longitudinal and transverse diffusion coefficients. Such may be the case in situ where it has been proposed (Cheng et al., 1996) that anisotropic arrangement of intracellular organelles (e.g., mitochondria) might restrict transverse diffusion.

For a reduced SR release of 1×10^{-19} moles, the peak values of [Ca], shown in Fig. 6, are reduced to a little less than half at the center of the cleft to about one-eighth at the M-line: ~3 mM at the center of the cleft, 15 μM at the outer radius of the cleft, 1 μM at the outer radius of the sarcomere in the Z-line plane, 0.25 μM at the M-line, and 1 μM averaged over the sarcomere volume. Comparing Figs. 5 and 7, halving the Ca release has two major effects: 1) In the cleft the fraction removed from the cell via Na/Ca exchange increases almost twofold to 15%. This is due to maintained transport by the exchangers secondary to sustained high cleft [Ca] (Fig. 6 *A*) despite decreased release. 2) The average free [Ca] in the sarcomere at end-release decreases by almost 70%. This is consistent with the decrease found by Fabiato (1985) and is due not only to the low release but to the high level of Ca efflux from the cell via the exchangers (see above).

SPECIAL CASES

Fluo-3

To compare the predictions of the model to fluorescent dye measurements of [Ca] we added 100 μM fluo-3 (Kao et al., 1989; Shacklock et al., 1995; Cheng et al., 1996) to the

sarcoplasm. Doing this approximately doubles the buffering capacity of the sarcoplasm. The results are shown in Figs. 8 and 9 for a 2×10^{-19} mole release and in Figs. 10 and 11 for a 1×10^{-19} mole release. In the sarcoplasm in the immediate vicinity of the cleft exit, there is a small reduction in the [Ca]. Away from the exit there is a reduction in the [Ca] to about half its value in the absence of fluo-3, and a delay and broadening of the Ca transients which increases with increasing distance from the cleft to tens of milliseconds in the vicinity of the M-line.

In fluorescent dye measurements of [Ca], the [Ca] is inferred from the amount of Ca that is bound to the fluo-3. The model predicts a further broadening of the [Ca-fluo-3] transients (Figs. 8 *B* and 10 *B*) compared to the [Ca] transients (Figs. 8 *A* and 10 *A*). In this case, the broadening is more significant in the region near the exit of the cleft, where the peaks of the Ca transients are sharper. The presence of the fluo-3 also results in a slowing of the re-uptake by the SR (compare Figs. 9 and 11 with Figs. 5 *B* and 7). The use of fluorescent dye to measure [Ca], therefore, has two serious problems. First, it causes a decrease in the free [Ca] that one is attempting to measure and second, the [Ca-fluo-3] transient that is being used to deduce the [Ca] is broadened relative to the free [Ca] transient. Note (compare Figs. 3 *A* and 8 *A*) that fluo-3 reduces peak average sarcomeric [Ca] by >50% and increases the initial half-time for decrease about twofold.

It also should be pointed out that no experimental measurements at the present time are able to attain the spatial resolution necessary to detect the spatially localized peak concentrations that the model predicts. For example, a confocal microscopic measurement obtains a weighted average over a $0.4 \times 0.4 \times 0.8$ μm region (Cannell et al., 1994). This then is a third reason why an experimental measurement might not detect a [Ca] as large as the present model predicts could be present.

"L" channel entry

As stated in Results the [Ca] profile previously presented for the cleft was for "L" channel entry nine times that stated (2.7 versus 0.3 pA) (Langer and Peskoff, 1996). The more physiological entry and resultant cleft [Ca] profile is now presented in Fig. 12. Though the calculated [Ca] is less by a factor of almost ten all nine feet within a 50 nm domain of an "L" channel will "see" a minimum 1 μM [Ca] within 1 ms (Fig. 12). According to Fabiato (1985) this concentration increase within this time will release an amount of Ca sufficient to activate 50% maximum force. As modeled previously (Langer and Peskoff, 1996) "reverse" Na/Ca exchange requires 10 ms to raise [Ca] to 0.5 μM, which would produce <20% maximum force. Thus channel entry is capable of generating twice the [Ca] in 10% of the time required for "reversed" Na/Ca exchange and therefore, if the model is correct, Fabiato's results would indicate that it serves as a more effective "trigger". This is the same conclusion reached previously (Langer and Peskoff, 1996).

Fig. 13 is a "snapshot" of [Ca] on the shaded plane in Fig. 1 outside the cleft 30 ms after "L" channel opening (no SR release). Such release produces trivial increases in [Ca], much below the level required to produce a discernible "spark" (Santana et al., 1996).

"Sparks"

To relate our model to experiments that measure "Ca sparks" we note that, even taking into account the distortions inherent in the fluorescent dye measurements, the [Ca] that we compute for the maximum-force SR release (and also half that release), leads to [Ca] too large to be interpreted as a spark. An SR release of 4×10^{-20} moles (20% of maximum release) over a 2-ms time period yields a [Ca] distribution in the sarcomere that could be classified as a spark (Fig. 14) (Santana et al., 1996). It has a peak [Ca] of 3 μM at the exit of the cleft, dropping to 1 μM an axial distance of 125 nm from the exit and to 200 nM at an axial distance of 600 nm. If 100 μM fluo-3 is added to the sarcoplasm, the peak [Ca] is reduced to slightly less than 3 μM, drops to 1 μM within an axial distance of ~50 nm from the cleft exit and to 200 nM at an axial distance of 300 nm (Fig. 15). Comparing Fig. 14 *C* (no fluo-3) and Fig. 15 *D* (100 μM fluo-3) it is seen that the dye "shrinks" the spark.

Sparks have recently been cited as "elementary events underlying excitation-contraction coupling" (Santana et al., 1996). In the original paper (Cheng et al., 1993) describing them it is stated, "The calcium spark is the *consequence* (our emphasis) of elementary events underlying excitation-contraction coupling." We would agree with the original de-
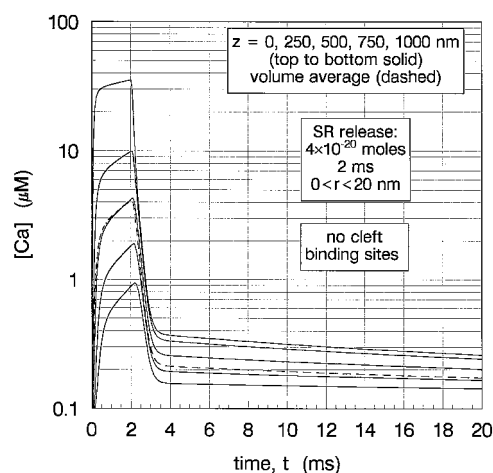

FIGURE 18　[Ca] versus *t* at the eight radially spaced points in the *z* = 0 plane shown in Fig. 1, for an SR release of 4×10^{-20} moles in a 2-ms-duration pulse. All conditions are identical to those in Fig. 14 *B*, except that the high- and low-affinity Ca binding sites have been deleted from the cleft. This deletion 1) increases [Ca] within the sarcomere at end-release by >10-fold; 2) causes average [Ca] to return to 200 nM within 2 ms as compared to 20 ms; 3) decreases the latency for spark appearance to ~100 μs from ~5 ms; 4) reduces the total spark duration to ~5 ms from >30 ms.
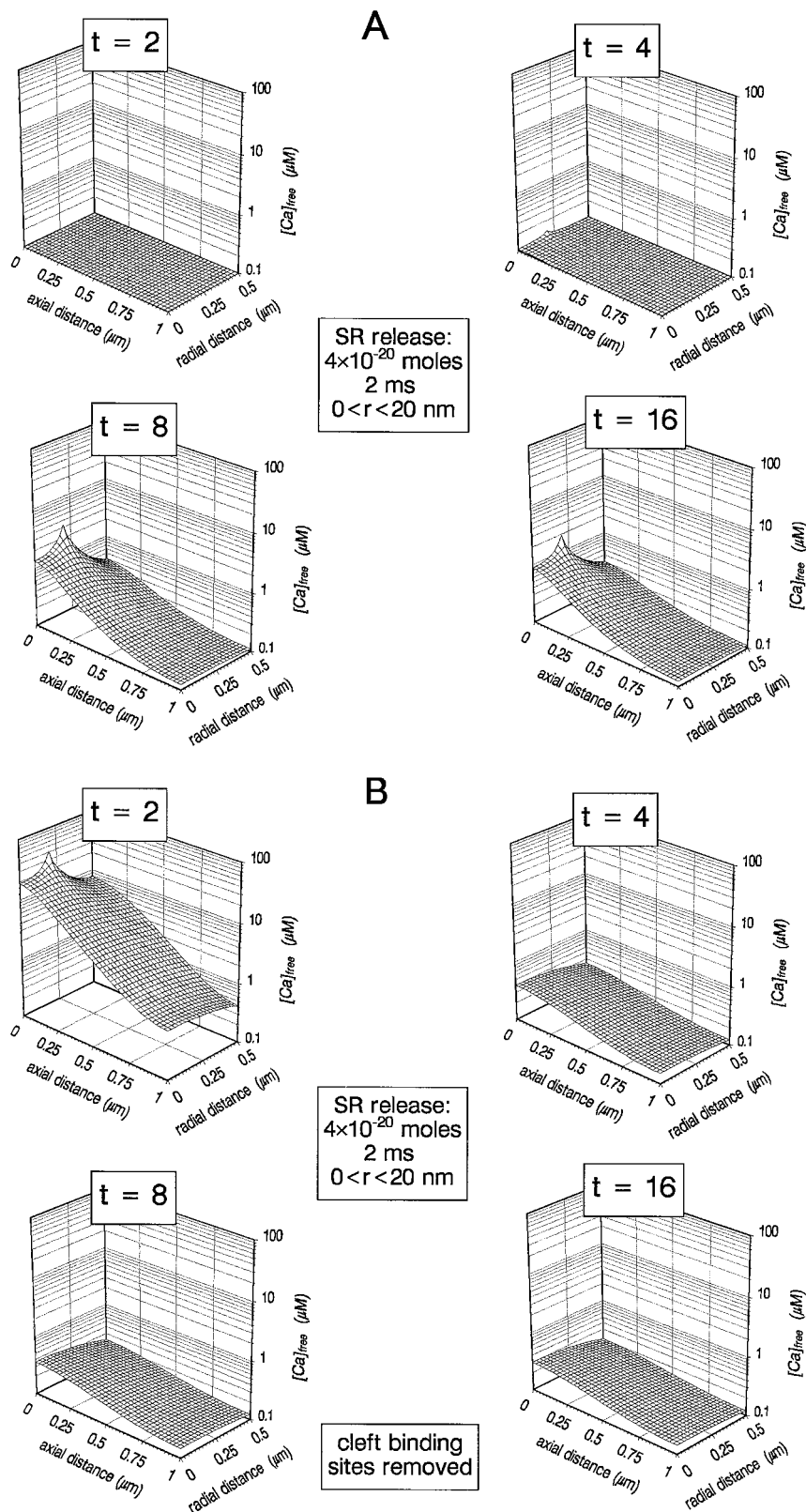
FIGURE 19   [Ca] snapshots at 2, 4, 8, and 16 ms for an SR release of 4×10^{-20} moles in a 2-ms-duration pulse. (*A*) With and (*B*) without binding sites in the cleft. Note that at $t = 4$ ms, in *A* the response is just beginning to appear, whereas in *B* it has already decreased by two orders of magnitude from its peak.

scription and our results suggest that the region of the cell where the "elementary events" occur is the diadic cleft. Perhaps the opening of a single ryanodine receptor channel (or a small cluster of receptors) is the elementary event. The

role of the cleft in transforming the release event and thereby determining the spark configuration is strikingly illustrated by comparison of Figs. 14 *B* and 18. All conditions for both figures are identical except that we have

deleted the high and low affinity Ca binding sites from the inner sarcolemmal leaflet (Post and Langer, 1992; Langer and Peskoff, 1996) within the diadic cleft. Note that this deletion: 1) increases [Ca] within the sarcomere by >10-fold at end release (average [Ca] rises to 4 μM as compared to 0.3 μM); 2) causes average [Ca] to return to 200 nM within 2 ms as compared to 20 ms; 3) decreases the latency for spark appearance to a few hundred microseconds from 4–5 ms; 4) reduces the total spark duration to ~5 ms from >30 ms. In fact, the spark would be essentially finished, in the absence of cleft sarcolemmal binding, before it would start in the presence of binding.

Comparison of [Ca] free "snapshots" at 2, 4, 8, and 16 ms with (Fig. 19 *A*) and without (Fig. 19 *B*) binding emphasizes the preceding points. The fact that sparks are routinely identified with present confocal microscopic techniques and appear as they do is due, in large measure, to the diffusional delays within the diadic cleft. These delays are, in turn, ascribable to the presence of the previously described sarcolemmal Ca-binding sites (Post et al., 1988; Post and Langer, 1992; Peskoff et al., 1992; Langer and Peskoff, 1996). Not only do these cleft sites play a significant role in determining the profile of the sarcomeric [Ca] transient but they are responsible for greatly increasing the efficiency of cellular Na/Ca exchange as has been recently documented (Wang et al., 1996).

"Corbular SR"

We have investigated the possibility that a part of the SR release occurs at a location outside the cleft, from the corbular SR, located in a ring at the outer cylindrical surface of the sarcomere, $r = b = 500$ nm, at an axial distance $z = 400$ nm from the Z-line. The total release amount is 2×10^{-19} moles during a 20-ms period, half from the JSR during the first 10 ms, and half from the CSR during the second 10 ms. The divided release is based on the assumption that SR content is proportional to the distribution of calsequestrin in JSR and CSR. Jorgensen et al., (1985) report a 60–40% distribution respectively. As compared to all release within the cleft, CSR release produces a superimposed 2–3 μM peak which subsides over ~10 ms and a moderate elevation of [Ca] in the sarcomere through the course of the transient (Figs. 2 *A*, 16, 4 *A*, 17). It is unlikely that current measurement of fluorescent response by confocal microscopy would be sufficient to resolve a separate CSR release (Pratusevich and Balke, 1996).

REFERENCES

Bassani, J. W., R. A. Bassani, and D. M. Bers. 1994. Relaxation in rabbit and rat cardiac cells: species-dependent differences in cellular mechanisms. *J. Physiol. (Lond.).* 476:279–293.

Cannell, M. B., H. Cheng, and W. J. Lederer. 1994. Spatial nonuniformities in [Ca^{2+}]$_i$ during excitation-contraction coupling in cardiac myocytes. *Biophys. J.* 67:1942–1956.

Cheng, H., W. J. Lederer, and M. B. Cannell. 1993. Calcium sparks: Elementary events underlying excitation-contraction coupling in heart muscle. *Science.* 262:740–744.

Cheng, H., M. R. Lederer, R.-P. Xiao, A. M. Gómez, Y.-Y Zhou, B. Ziman, H. Spurgeon, E. G. Lakatta, and W. J. Lederer. 1996. Excitation-contraction coupling in heart: new insights from Ca^{2+} sparks. *Cell Calcium.* 20:129–140.

Crank, J. 1975. The Mathematics of Diffusion, 2nd Ed. Clarendon Press, Oxford.

Dolber, P. C., and J. R. Sommer. 1984. Corbular sarcoplasmic reticulum of rabbit cardiac muscle. *J. Ultrastruct. Res.* 87:190–196.

Escobar, A. L., F. Cifuentes, and J. Vergara. 1995. Detection of Ca^{+2} transients elicited by photolysis of DM-nitrophen with a fast calcium indicator. *FEBS Lett.* 364:335–338.

Fabiato, A. 1985. Time and calcium dependence of activation and inactivation of calcium-induced release of calcium from the sarcoplasmic reticulum of a skinned canine cardiac Purkinje cell. *J. Gen. Physiol.* 85:247–289.

Frank, J. S., G. Mottino, D. Reid, R. S. Molday, and K. D. Philipson. 1992. Distribution of the Na^+-Ca^{2+} exchanger protein in mammalian cardiac myocytes: an immuno-fluorescence and immunocolloidal gold-labeling study. *J. Cell. Biol.* 117:337–345.

Isenberg, G., E. F. Etter, M.-F. Wendt-Gallitelli, A. Schiefer, W. A. Carrington, R. A. Tuft, and F. S. Fay. 1996. Intra-sarcomere [Ca^{2+}] gradients in ventricular myocytes revealed by high speed digital imaging microscopy. *Proc. Natl. Acad. Sci. USA.* 93:5413–5418.

Jorgensen, A. O., A. C.-Y. Shen, and K. P. Campbell. 1985. Ultrastructural localization of calsequestrin in adult rat atrial and ventricular muscle cells. *J. Cell. Biol.* 101:257–268.

Kao, J. P. Y., A. T. Harootunian, and R. Y. Tsien. 1989. Photochemically generated cytosolic calcium pulses and their detection by fluo-3. *J. Biol. Chem.* 264:8179–8184.

Langer, G. A., and A. Peskoff. 1996. Calcium concentration and movement in the diadic cleft space of the cardiac ventricular cell. *Biophys. J.* 70:1169–1182.

Levitsky, D. O., D. S. Benevalensky, T. S. Levchenko, V. N. Smirnov, and E. I. Chazov. 1981. Calcium binding rate and capacity of cardiac sarcoplasmic reticulum. *J. Mol. Cell. Cardiol.* 13:785–796.

Luo, C. H., and Y. Rudy 1994. A dynamic model of the cardiac ventricular action potential. I. Simulations of ionic current and concentration changes. *Circ. Res.* 74:1071–1096.

Matsuoka, S., and D. Hilgemann. 1992. Steady-state and dynamic properties of cardiac sodium-calcium exchange. Ion and voltage dependencies of the transport cycle. *J. Gen. Physiol.* 100:963–1001.

Minta, A., J. P. Y. Kao, and R. Y. Tsien. 1989. Fluorescent indicators for cytosolic calcium based on rhodamine and fluorescein chromophores. *J. Biol. Chem.* 264:8171–8178.

Nowycky, M. C., and M. J. Pinter. 1993. Time course of Ca^{2+} and Ca^{2+}-bound buffers following Ca^{2+} influx in a model cell. *Biophys. J.* 64:77–91.

Peskoff, A., J. A. Post, and G. A. Langer. 1992. Sarcolemmal calcium binding sites in heart. II. Mathematical model for diffusion of calcium released from the sarcoplasmic reticulum into the diadic region. *J. Membr. Biol.* 129:59–69.

Post, J. A., and G. A. Langer. 1992. Sarcolemmal calcium binding sites in heart. I. Molecular origin in "gas-dissected" sarcolemma. *J. Membr. Biol.* 129:48–57.

Post, J. A., G. A. Langer, J. A. F. Opden Kamp, and A. J. Verkleij. 1988. Phospholipid asymmetry in cardiac sarcolemma. Analysis of intact cells and "gas dissected" membranes. *Biochim. Biophys. Acta.* 943:256–266.

Pratusevich, V. R., and C. W. Balke. 1996. Factors shaping the confocal image of the calcium spark in cardiac muscle cells. *Biophys. J.* 71:2942–2957.

Radermacher, M., V. Rao, R. Grassuci, J. Frank, A. P. Timerman, S. Fleischer, and T. Wagenknecht. 1994. Cryo-elctron microscopy and

three dimensional reconstruction of the calcium release channel/ryanodine receptor from skeletal muscle. *J. Cell. Biol.* 127:411–423.

Rousseau, E., and G. Meissner. 1989. Single cardiac sarcoplasmic reticulum Ca^{2+} release channel: activation by caffeine. *Am. J. Physiol.* H328–H333.

Rousseau, E., J. S. Smith, J. S. Henderson, and G. Meissner. 1986. Single channel and $^{45}Ca^{2+}$ flux measurements of the cardiac sarcoplasmic reticulum calcium channel. *Biophys. J.* 50:1009–1014.

Santana, L. F., H. Cheng, A. M. Gómez, M. B. Cannell, and W. J. Lederer. 1996. Relation between the sarcolemmal Ca^{2+} current and Ca^{2+} sparks and local control theories for cardiac excitation-contraction coupling. *Circ. Res.* 78:166–171.

Schouten, V. J. A., and H. terKeurs. 1985. The slow repolarization phase of the action potential in rat heart. 1985. *J. Physiol. (Lond.).* 360:13–35.

Shacklock, P. S., W. G. Wier, and C. W. Balke. 1995. Local Ca^{2+} transients (Ca^{2+} sparks) originate at transverse tubules in rat heart cells. *J. Physiol. (Lond.).* 487:601–608.

Sipido, K. R., and W. G. Wier. 1991. Flux of Ca^{2+} across the sarcoplasmic reticulum of guinea-pig cardiac cells during excitation-contraction coupling. *J. Physiol. (Lond.).* 435:605–630.

Smith, G. D., J. Wagner, and J. Keizer. 1996. Validity of the rapid buffering approximation near a point source of calcium ions. *Biophys. J.* 70:2527–2539.

Spurgeon, H. A., M. D. Stern, G. Baartz, S. Raffaeli, R. G. Hansford, A. Talo, E. G. Lakatta, and M. C. Capogrossi. 1990. Simultaneous measurement of Ca^{2+}, contraction, and potential in cardiac myocytes. *Am. J. Physiol.* 258:H574–H586.

Takamatsu, T., and W. G. Wier. 1990. Calcium waves in mammalian heart: quantification of origin, magnitude, waveform and velocity. *FASEB J.* 4:1519–1525.

Wang, S.-Y., A. Peskoff, and G. A. Langer. 1996. Inner sarcolemmal leaflet Ca^{2+} binding: its role in cardiac Na/Ca exchange. *Biophys. J.* 70:2266–2274.

Wibo, M., G. Bravo, and T. Godfraind. 1991. Postnatal maturation of excitation-contraction coupling in rat ventricle in relation to the subcellular localization and surface density of 1,4-hydropyridine and ryanodine receptors. *Circ. Res.* 68:662–673.

Wier, W. G., and D. T. Yue. 1986. Intracellular calcium transients underlying the short-term force-interval relationship in ferret ventricular myocardium. *J. Physiol. (Lond.).* 376:507–530.